

A Benchmark to Sparse Coding: When Group Sparsity Meets Rank Minimization

Zhiyuan Zha, *Member, IEEE*, Xin Yuan, *Senior Member, IEEE*, Bihan Wen, *Member, IEEE*, Jiantao Zhou, *Member, IEEE*, Jiachao Zhang, *Member, IEEE* and Ce Zhu, *Fellow, IEEE*

Abstract—Sparse coding has achieved a great success in various image processing studies. However, a benchmark to measure the sparsity of image patch/group is missing since the sparse coding is essentially an NP-hard problem. In this paper, we present a benchmark to sparse coding from the perspective of rank minimization. We firstly design an adaptive dictionary to bridge the gap between the group-based sparse coding (GSC) and rank minimization. Then, we prove that under the designed dictionary, GSC and the rank minimization problems are equivalent to each other, and therefore the sparse coefficients of each patch group can be measured by estimating the singular values of each patch group. Based on this scheme, we thus earn a benchmark to measure the sparsity of each patch group because the singular values of the original image patch groups can be easily computed by the singular value decomposition (SVD) operator. This benchmark can be used to evaluate the performance of any kind of norm minimization methods in sparse coding. Then, we can evaluate different norm minimization methods in sparse coding through analyzing their corresponding rank minimization counterparts. Specifically, we exploit four well-known rank minimization methods to analyze the sparsity of each patch group and the weighted Schatten p -norm minimization (WSNM) is found to be the closest one to the real singular values of each patch group. Inspired by the aforementioned equivalence of the rank minimization and GSC regime, WSNM can be translated into a non-convex weighted ℓ_p -norm minimization problem in GSC, and based on the earned benchmark in sparse coding, the weighted ℓ_p -norm minimization is expected to obtain better performance than the other three norm minimization methods. To verify the feasibility of the proposed benchmark, we compare the weighted ℓ_p -norm minimization with the other three norm minimization methods in sparse coding. Experimental results on two image restoration applications, namely image inpainting and image compressive sensing recovery, demonstrate that the proposed scheme is feasible and outperforms many state-of-the-art methods.

Index Terms—Sparse coding, GSC, rank minimization, adaptive dictionary, weighted ℓ_p -norm minimization, image restoration.

I. INTRODUCTION

Z. Zha and C. Zhu are with the School of Information and Communication Engineering, University of Electronic Science and Technology of China, Chengdu, 611731, China. E-mail: zhazhiyuan.mmd@gmail.com, eczhu@uestc.edu.cn.

X. Yuan is with Nokia Bell Labs, 600 Mountain Avenue, Murray Hill, NJ, 07974, USA. E-mail: xyuan@bell-labs.com.

B. Wen is with School of Electrical and Electronic Engineering, Nanyang Technological University, Singapore 639798. E-mail: bihan.wen@ntu.edu.sg.

J. Zhou is with Department of Computer and Information Science, University of Macau, Macau 999078, China. E-mail: jtzhou@umac.mo.

J. Zhang is with Kangni Mechanical and Electrical Institute, Nanjing Institute of Technology, Nanjing 211167, China. E-mail: zhangjc07@foxmail.com.

TRADITIONAL patch-based sparse coding (PSC) has been widely used in various image processing tasks and has achieved excellent results [1–4]. It assumes that each patch of an image can be precisely modeled by a sparse linear combination of some fixed and trainable basis elements, which are called atoms and these atoms compose a dictionary. As such, one key issue in sparse coding based scheme is to train a dictionary, with popular techniques including K-SVD [1], ODL [3] and SDL [4]. However, there exists two main issues in the PSC model. *i)* Since dictionary learning is a large-scale and highly non-convex problem, it is computationally expensive. *ii)* The PSC model usually assumes the independence of image patches, which does not take account of the correlation between similar patches [5–8].

To overcome the aforementioned limitations, instead of using a single patch as the basic unit in sparse coding, recent advances of group-based sparse coding (GSC) consider similar *patch group* as the basic unit and have demonstrated great potentials in various image processing tasks [5–13]. The GSC is a powerful mechanism to integrate intrinsic local sparsity and nonlocal self-similarity (NSS) of images [5]. Specifically, taking an (vectorized) image $\mathbf{x} \in \mathbb{R}^N$ as an example, it is divided into n overlapped patches of size $\sqrt{d} \times \sqrt{d}$, and each patch is denoted by a vector $\mathbf{x}_i \in \mathbb{R}^d$, $i = 1, 2, \dots, n$. Then for each patch \mathbf{x}_i , m similar matched patches are selected from a searching window with $C \times C$ pixels to form a set \mathcal{S}_i . It is noticed that K-Nearest Neighbour (KNN) algorithm [14] is usually utilized to search similar matched patches. Following this, all patches in \mathcal{S}_i are stacked into a matrix $\mathbf{X}_i \in \mathbb{R}^{d \times m}$, *i.e.*, $\mathbf{X}_i = \{\mathbf{x}_{i,1}, \mathbf{x}_{i,2}, \dots, \mathbf{x}_{i,m}\}$. This matrix \mathbf{X}_i consisting of patches with similar structures is thereby called a patch group, where $\{\mathbf{x}_{i,j}\}_{j=1}^m$ denotes the j -th patch in the i -th patch group. Similar to PSC [1, 2], given a dictionary \mathbf{D}_i , each patch group \mathbf{X}_i can be sparsely represented by solving the following ℓ_0 -norm minimization problem,

$$\hat{\mathbf{A}}_i = \arg \min_{\mathbf{A}_i} \left(\frac{1}{2} \|\mathbf{X}_i - \mathbf{D}_i \mathbf{A}_i\|_F^2 + \lambda \|\mathbf{A}_i\|_0 \right), \quad (1)$$

where \mathbf{A}_i represents the group sparse coefficient of each patch group \mathbf{X}_i and λ is a regularization parameter. $\|\cdot\|_F$ denotes the Frobenius norm, and $\|\cdot\|_0$ signifies the ℓ_0 -norm, *i.e.*, counting the nonzero entries of each column in \mathbf{A}_i . Then the entire image \mathbf{x} can be sparsely represented by a set of group sparse codes $\{\mathbf{A}_i\}_{i=1}^n$.

It is well-known that norm minimization methods are often used to evaluate the sparsity of a signal/image [15–22]. However, since ℓ_0 -norm minimization problem is a difficult

combinatorial optimization, solving Eq. (1) is NP-hard. For this reason, it is often replaced by the ℓ_1 -norm minimization [15] to make the optimization problem tractable. Meanwhile, advanced norm minimization methods, like the weighted ℓ_1 -norm minimization [16], the $\ell_{1/2}$ -norm minimization [17] and the weighted $\ell_{2,1}$ -norm minimization [18], are also proposed to solve the ℓ_0 -norm minimization problem. Unfortunately, for some practical problems, such as image inverse problems [5–7, 9], no matter which method is used, it is just an *estimate* to the ℓ_0 -norm minimization and cannot obtain the real sparse solution. During the past decades, there are still existing many arguments about which one is the best sparsity of these norm minimization methods [16–22]. More importantly, although we possess the original signal/image \mathbf{x} , it is almost impossible to obtain the real solution of each group sparse coefficient A_i in Eq. (1), due to the NP-hard essence of the ℓ_0 -norm minimization problem. Furthermore, the dictionary plays a pivot role in estimation of each group sparse coefficient A_i in Eq. (1), but the dictionary can have many different design methods. Therefore, a benchmark to sparse coding is desired to measure the sparsity of a signal/image.

Bearing the above concerns in mind, this paper provides a benchmark to sparse coding from the point of rank minimization. To the best of our knowledge, this is the first work to propose a benchmark for sparse coding. The contributions of our paper are as follows.

- 1) An adaptive dictionary for each patch group is designed to bridge the gap between the GSC and rank minimization models.
- 2) Based on this dictionary learning scheme, we prove the equivalence of the GSC and rank minimization models, and thus the sparse coefficients of each patch group can be measured by calculating the singular values of each patch group. Therefore, under this scheme, a benchmark is earned to measure the sparsity of each patch group since the singular values of the original image patch groups can be easily obtained by the singular value decomposition (SVD) operator. Then, we can apply this benchmark to evaluate the performance of any kind of norm minimization methods in sparse coding. In other words, we can measure different norm minimization methods in sparse coding through analyzing their corresponding rank minimization counterparts.
- 3) Four well-known rank minimization methods, *i.e.*, standard nuclear norm minimization (NNM) [23], Schatten p -norm minimization (SNM) [24], weighted nuclear norm minimization (WNNM) [25] and the weighted Schatten p -norm minimization (WSNM) [26], are used to analyze the sparsity of each patch group¹ and the solution of WSNM is found to be the nearest one to the real singular values of each patch group, please refer to Figs. 1-2 for a demonstration.
- 4) Inspired by the equivalence of the rank minimization and GSC, NNM, SNM, WNNM and WSNM can be equivalently translated into ℓ_1 -norm minimization, ℓ_p -

norm minimization, weighted ℓ_1 -norm minimization and the weighted ℓ_p -norm minimization problems in GSC, respectively. Then, based on the earned benchmark in sparse coding, the weighted ℓ_p -norm minimization is expected to obtain higher performance than the other three norm minimization methods.

- 5) To verify the feasibility of the proposed benchmark, the weighted ℓ_p -norm minimization is used to compare with the other three norm minimization methods under the GSC framework². To make the proposed scheme tractable and robust, the alternating direction method of multipliers (ADMM) framework is developed to solve the non-convex weighted ℓ_p -norm minimization problem. Experimental results on image inpainting and image compressive sensing (CS) recovery applications, show that the proposed scheme is feasible and outperforms many state-of-the-art methods in both objective and perceptual quality.

The rest of this paper is organized as follows. Section II briefly reviews the rank minimization methods and some nuclear norms. Section III introduces the adaptive dictionary learning approach and presents the proposed benchmark to sparse coding from the perspective of rank minimization. Section IV develops an efficient algorithm to solve the weighted ℓ_p -norm minimization problem based on the ADMM framework. Section V presents experimental results and Section VI concludes the entire paper. The preliminary version of this work has appeared in [33]³.

II. BACKGROUND AND RELATED WORK

A. Rank Minimization Methods

The main goal of low-rank matrix approximation (LRMA) is to recover the underlying low-rank structure of a matrix from its degraded/corrupted observation. In general, methods of LRMA can be classified into two categories: the low-rank matrix factorization (LRMF) methods [34–36] and the rank minimization methods [23–32]. In this work we focus on the *rank minimization* problem. To be concrete, for an input matrix \mathbf{Y} , the rank minimization approach aims to find a low-rank matrix \mathbf{X} , which is as close to \mathbf{Y} as possible under the F -norm data fidelity term with a nuclear norm constraint,

$$\hat{\mathbf{X}} = \arg \min_{\mathbf{X}} \left(\frac{1}{2} \|\mathbf{Y} - \mathbf{X}\|_F^2 + \lambda \mathbf{R}(\mathbf{X}) \right), \quad (2)$$

where λ is a parameter to balance the loss function and the low-rank regularization induced by the nuclear norm $\mathbf{R}(\mathbf{X})$, which will be introduced in the following subsection.

²Note that the proposed benchmark is suitable for traditional PSC model, since the GSC is the generalized form of the PSC (when similar matched patches $m = 1$).

³Significant changes have been made compared to our previous work in [33]. Specifically, we have added the analysis of the proposed benchmark using the rank minimization methods in Sec. III-C. The gradient descent algorithm is introduced in Sec. IV-A1 to solve the CS recovery problem. Extensive experimental results have been added to verify the feasibility, robustness, and convergence of the proposed algorithm in Sec. V.

¹Some other rank minimization methods [27–33] can also be used to analyze the sparsity of each patch group.

B. Nuclear Norms

Hereby, we briefly introduce four well-known nuclear norms, including standard nuclear norm [23], Schatten p -norm [24], weighted nuclear norm [25] and the weighted Schatten p -norm [26].

Definition 1. A widely used **standard nuclear norm** [23] of a matrix \mathbf{X} can be expressed as

$$\|\mathbf{X}\|_* = \sum_{i=1}^{\min\{d,m\}} \sigma_i = \text{Tr}((\mathbf{X}^T \mathbf{X})^{\frac{1}{2}}), \quad (3)$$

where σ_i is the i -th singular value of \mathbf{X} and $\text{Tr}(\cdot)$ calculates the trace of the matrix in (\cdot) .

Definition 2. The **Schatten p -norm** [24] of a matrix \mathbf{X} can be expressed as

$$\|\mathbf{X}\|_{S_p} = \left(\sum_{i=1}^{\min\{d,m\}} \sigma_i^p \right)^{\frac{1}{p}} = \left(\text{Tr}((\mathbf{X}^T \mathbf{X})^{\frac{p}{2}}) \right)^{\frac{1}{p}}, \quad (4)$$

where $0 < p \leq 1$, and σ_i is the i -th singular value of \mathbf{X} .

Definition 3. The **weighted nuclear norm** [25] of a matrix \mathbf{X} can be expressed as

$$\|\mathbf{X}\|_{\mathbf{w},*} = \left(\sum_{i=1}^{\min\{d,m\}} w_i \sigma_i \right) = \text{Tr}(\mathbf{W}\mathbf{\Sigma}), \quad (5)$$

where $\mathbf{w} = [w_1, \dots, w_{\min\{d,m\}}]$, σ_i is the i -th singular value of \mathbf{X} and $w_i \geq 0$ is a weight assigned to σ_i . \mathbf{W} and $\mathbf{\Sigma}$ are diagonal matrices whose diagonal entries are composed of w_i and σ_i , respectively.

Definition 4. The **weighted Schatten p -norm** [26] of a matrix \mathbf{X} is

$$\|\mathbf{X}\|_{\mathbf{w},S_p} = \left(\sum_{i=1}^{\min\{d,m\}} w_i \sigma_i^p \right)^{\frac{1}{p}}, \quad (6)$$

where $0 < p \leq 1$, and σ_i is the i -th singular value of \mathbf{X} . $\mathbf{w} = [w_1, \dots, w_{\min\{d,m\}}]$ and $w_i \geq 0$ is a weight assigned to σ_i .

The weighted Schatten p -norm of \mathbf{X} with **power p** is

$$\|\mathbf{X}\|_{\mathbf{w},S_p}^p = \sum_{i=1}^{\min\{d,m\}} w_i \sigma_i^p = \text{Tr}(\mathbf{W}\mathbf{\Sigma}^p), \quad (7)$$

where \mathbf{W} and $\mathbf{\Sigma}$ are diagonal matrices whose diagonal entries are composed of w_i and σ_i , respectively.

III. A BENCHMARK TO SPARSE CODING BASED ON THE RANK MINIMIZATION METHODS

We hereby present a benchmark to sparse coding from the point of rank minimization. Towards this end, an adaptive dictionary for each patch group is designed to bridge the gap between the GSC and rank minimization models. Rested on this dictionary learning scheme, we prove that GSC is equivalent to the rank minimization problem, and then the sparse coefficients in each patch group can be measured by calculating the singular values of each patch group. Thereby, we have a benchmark to measure the sparsity of each patch group via the rank minimization since the singular values of the original image patch groups can be easily obtained by

the SVD operator⁴. This benchmark can be used to compare the performance of any kind of norm minimization methods in sparse coding. We can thus measure different norm minimization methods in sparse coding through analyzing their corresponding rank minimization counterparts. In this way, we have achieved a clear visual comparison to analyze the sparsity of each patch group, please refer to Figs. 1-2 for a demonstration.

A. Adaptive Dictionary Learning

An adaptive dictionary learning approach is now designed, that is, for each patch group \mathbf{X}_i , its adaptive dictionary can be learned from its observation $\mathbf{Y}_i \in \mathbb{R}^{d \times m}$. Specifically, we apply the SVD to \mathbf{Y}_i ,

$$\mathbf{Y}_i = \mathbf{U}_i \mathbf{\Delta}_i \mathbf{V}_i^T = \sum_{j=1}^{n_1} \delta_{i,j} \mathbf{u}_{i,j} \mathbf{v}_{i,j}^T, \quad (8)$$

where $\mathbf{\Delta}_i = \text{diag}(\delta_{i,1}, \delta_{i,2}, \dots, \delta_{i,n_1})$ is a diagonal matrix, $n_1 \stackrel{\text{def}}{=} \min(d, m)$, and $\mathbf{u}_{i,j}, \mathbf{v}_{i,j}$ are the columns of \mathbf{U}_i and \mathbf{V}_i , respectively.

Following this, we define each dictionary atom $\mathbf{d}_{i,j}$ of the adaptive dictionary \mathbf{D}_i for every patch group \mathbf{Y}_i , i.e.,

$$\mathbf{d}_{i,j} = \mathbf{u}_{i,j} \mathbf{v}_{i,j}^T, \quad j = 1, 2, \dots, n_1. \quad (9)$$

Till now, we have learned an adaptive dictionary, i.e.,

$$\mathbf{D}_i = [\mathbf{d}_{i,1}, \mathbf{d}_{i,2}, \dots, \mathbf{d}_{i,n_1}]. \quad (10)$$

It can be seen that the designed dictionary learning approach only requires one SVD operation per patch group.

B. Prove the equivalence of Group-based Sparse Coding and Rank Minimization Problem

In order to present the proposed benchmark to sparse coding, we first prove that GSC is equivalent to the rank minimization models based on the designed dictionary, and we need the following conclusions.

Lemma 1. The minimization problem

$$\hat{\mathbf{x}} = \arg \min_{\mathbf{x}} \left(\frac{1}{2} \|\mathbf{x} - \mathbf{a}\|_2^2 + \tau \|\mathbf{x}\|_1 \right), \quad (11)$$

has a closed-form solution

$$\hat{\mathbf{x}} = \text{soft}(\mathbf{a}, \tau) = \text{sgn}(\mathbf{a}) \odot \max(\text{abs}(\mathbf{a}) - \tau, 0), \quad (12)$$

where \odot denotes the element-wise (Hadamard) product.

Proof. See [41]. □

Consider the SVD of a matrix $\mathbf{Y} \in \mathbb{R}^{d \times m}$ with rank r ,

$$\mathbf{Y} = \mathbf{U} \mathbf{\Delta} \mathbf{V}^T, \quad \mathbf{\Delta} = \text{diag}(\{\delta_i\}_{1 \leq i \leq r}), \quad (13)$$

where $\mathbf{U} \in \mathbb{R}^{d \times r}$ and $\mathbf{V} \in \mathbb{R}^{m \times r}$ are orthogonal matrices; δ_i is the i -th singular value of \mathbf{Y} . For any $\lambda \geq 0$, the soft-thresholding operator \mathcal{D}_λ is defined as

$$\mathcal{D}_\lambda(\mathbf{Y}) = \mathbf{U} \mathcal{D}_\lambda(\mathbf{\Delta}) \mathbf{V}^T, \quad \mathcal{D}_\lambda(\mathbf{\Delta}) = \text{soft}(\delta_i, \lambda). \quad (14)$$

⁴Note that the singular values have clear physical meanings in various practical problems [25, 37, 38]. The SVD operator of an object is more able to reflect its essential property than some estimation algorithms, such as Hard-Thresholding [39] and OMP [40].

Then, we have the following Theorem.

Theorem 1. For any $\lambda \geq 0$ and $\mathbf{Y} \in \mathbb{R}^{d \times m}$, the singular value shrinkage operator in Eq. (14) satisfies

$$\mathcal{D}_\lambda(\mathbf{Y}) = \arg \min_{\mathbf{X}} \left(\frac{1}{2} \|\mathbf{Y} - \mathbf{X}\|_F^2 + \lambda \|\mathbf{X}\|_* \right). \quad (15)$$

Proof. See [23]. \square

Recalling the adaptive dictionary defined in Eq. (10), and the classical ℓ_1 -norm minimization based GSC problem can be represented as

$$\hat{\mathbf{A}}_i = \arg \min_{\mathbf{A}_i} \left(\frac{1}{2} \|\mathbf{Y}_i - \mathbf{D}_i \mathbf{A}_i\|_F^2 + \lambda \|\mathbf{A}_i\|_1 \right). \quad (16)$$

According to the above design of the adaptive dictionary \mathbf{D}_i in Eq. (10), we have the following Lemma.

Lemma 2.

$$\|\mathbf{Y}_i - \mathbf{X}_i\|_F^2 = \|\mathbf{B}_i - \mathbf{A}_i\|_F^2, \quad (17)$$

where $\mathbf{Y}_i = \mathbf{D}_i \mathbf{B}_i$ and $\mathbf{X}_i = \mathbf{D}_i \mathbf{A}_i$.

Proof. See Appendix A. \square

Based on Lemmas 1-2 and Theorem 1, we have the following theorem.

Theorem 2. The equivalence of ℓ_1 -norm minimization based GSC and the NNM problems is satisfied under the designed adaptive dictionary \mathbf{D}_i , i.e.,

$$\begin{aligned} \hat{\mathbf{A}}_i &= \arg \min_{\mathbf{A}_i} \left(\frac{1}{2} \|\mathbf{Y}_i - \mathbf{D}_i \mathbf{A}_i\|_F^2 + \lambda \|\mathbf{A}_i\|_1 \right) \\ &\quad \Downarrow \\ \hat{\mathbf{X}}_i &= \arg \min_{\mathbf{X}_i} \left(\frac{1}{2} \|\mathbf{Y}_i - \mathbf{X}_i\|_F^2 + \lambda \|\mathbf{X}_i\|_* \right). \end{aligned} \quad (18)$$

Proof. See Appendix B. \square

Similar to Theorem 2, we have the following conclusion.

Corollary 1. Based on the designed adaptive dictionary \mathbf{D}_i , the weighted ℓ_1 -norm minimization based GSC, ℓ_p -norm minimization based GSC and the weighted ℓ_p -norm minimization based GSC problems are equivalent to WNNM, SNM and the WSNM problems, respectively.

Proof. See Appendix C. \square

Note that the dictionary can be learned in various manners and the designed adaptive dictionary learning approach is just one of them. The above conclusions cannot hold for some general dictionaries [3, 4, 42, 43]. Therefore, to further demonstrate the universality and advantage of the proposed scheme, another two generalized dictionary learning methods are also exploited to verify the feasibility of the proposed benchmark, i.e., graph-based dictionary learning method [42] and PCA dictionary learning method [43] (See subsection V-B for more details).

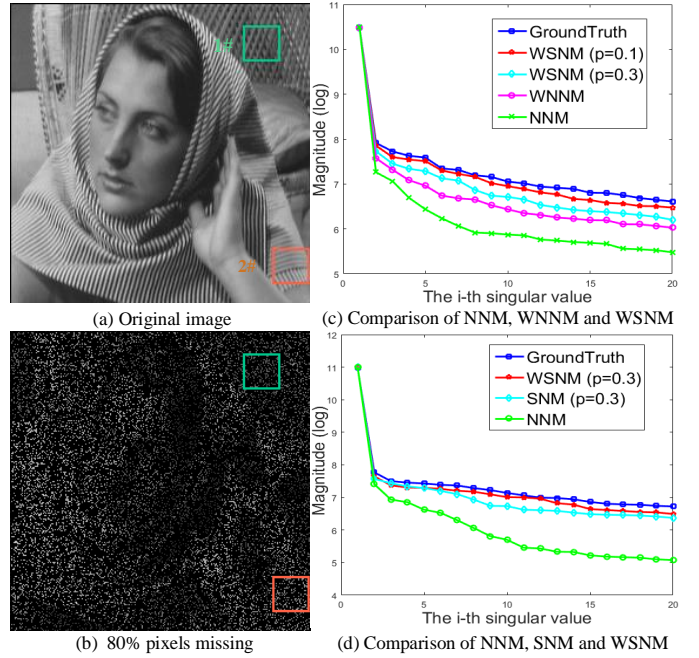


Fig. 1. Analyzing the sparsity of each patch group based on the rank minimization scheme in terms of image inpainting. (a) Original *Barbara* image. (b) 80% pixels are missing. (c-d) The curved lines of the singular values using different rank minimization methods of the patch group with reference in the cyan (1#) and orange (2#) boxes, respectively.

C. A Benchmark of Sparse Coding based on the Rank Minimization Methods

Based on Theorem 2 and Corollary 1, the GSC problem can be transformed into the rank minimization problem. We therefore possess a benchmark to measure the sparsity of each patch group via the rank minimization scheme because the singular values of the original image patch groups can be easily achieved by the SVD operator. Then, we can exploit the proposed benchmark to measure different norm minimization methods in sparse coding through analyzing their corresponding rank minimization methods.

Specifically, four well-known rank minimization methods are used to constrain Eq. (2) to analyze the sparsity of each patch group, i.e., NNM, SNM, WNNM and WSNM. In these experiments, two widely used images, namely, *Barbara* and *boats*, are used as examples in the context of image inpainting and image CS recovery, respectively. In image inpainting, 80% pixels of image *Barbara* are damaged in Fig. 1(b) and two patch groups based on 1# position and 2# position are generated in Fig. 1(a). In image CS recovery, image *boats* is compressively sampled by a random Gaussian matrix with $0.2N$ measurements and an initial image is estimated by using a standard CS recovery method (e.g., DCT/BCS [44] based CS reconstruction method) shown in Fig. 2(b). We conduct two patch groups based on 3# position and 4# position in Fig. 2(a). From Fig. 1(c-d) and Fig. 2(c-d), we can clearly observe that the singular values of the WSNM results are the best approximation to the ground-truth in comparison with the other three rank minimization methods, i.e., NNM, SNM and WNNM.

Based on Theorem 2 and Corollary 1, NNM, SNM, WNNM

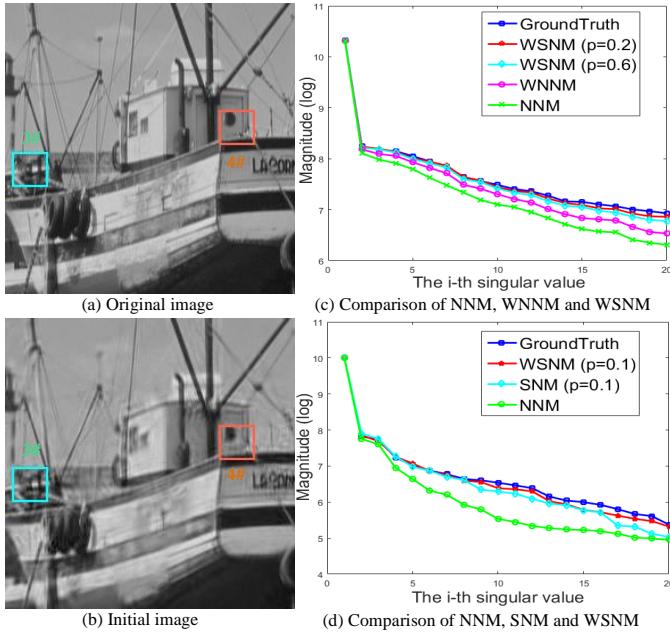


Fig. 2. Analyzing the sparsity of each patch group based on the rank minimization scheme in terms of image CS recovery. The image *boats* in (a) is compressively sampled by a random Gaussian matrix with $0.2N$ measurements, and an initial image in (b) is estimated by using the BCS based CS image recovery method [44]. (c-d) The curved lines of the singular values using different rank minimization methods of the patch group with reference in the cyan (3#) and orange (4#) boxes, respectively.

and WSNM can be equivalently transformed to ℓ_1 -norm minimization, ℓ_p -norm minimization, weighted ℓ_1 -norm minimization and the weighted ℓ_p -norm minimization problems in GSC, respectively. Meanwhile, based on the earned benchmark, *i.e.*, according to the above analysis of Fig. 1 and Fig. 2, we also wish that the weighted ℓ_p -norm minimization can achieve higher performance than the other three norm minimization methods in sparse coding, including ℓ_1 -norm minimization, ℓ_p -norm minimization and the weighted ℓ_1 -norm minimization. To verify the feasibility of the proposed benchmark, we compare the weighted ℓ_p -norm minimization with the other three norm minimization methods in sparse coding. Specifically, based on the GSC framework, we exploit these methods to solve two image restoration tasks including image inpainting and image CS recovery.

IV. VALIDATION OF THE BENCHMARK TO SPARSE CODING VIA THE WEIGHTED ℓ_p -NORM MINIMIZATION

According to the above analysis and based on our proposed benchmark in sparse coding, the weighted ℓ_p -norm minimization is expected to achieve better results than the other three norm minimization methods.

In this section, we apply two image restoration tasks including image inpainting and image CS recovery to verify the feasibility of the proposed benchmark. Specifically, the goal of image restoration [45–57] is to reconstruct a high quality image \mathbf{x} from its degraded observation \mathbf{y} ,

$$\mathbf{y} = \mathbf{H}\mathbf{x} + \mathbf{n}, \quad (19)$$

where \mathbf{H} is a non-invertible linear degradation operator and \mathbf{n} is usually assumed to be a zero-mean white Gaussian noise.

With different setting of matrix \mathbf{H} , Eq. (19) can represent different image restoration tasks. For instance, when \mathbf{H} is a diagonal matrix whose diagonal entries are either 1 or 0, keeping or killing corresponding pixels, Eq. (19) becomes image inpainting [47–51]; when \mathbf{H} is a random projection matrix with more columns than rows, Eq. (19) becomes image CS recovery [52–56].

Then, we exploit the case of the weighted ℓ_p -norm minimization as an example. Given the degraded image \mathbf{y} in Eq. (19), we aim to recover the original image \mathbf{x} by solving the following non-convex weighted ℓ_p -norm minimization problem,

$$\hat{\alpha} = \arg \min_{\alpha} \frac{1}{2} \|\mathbf{y} - \mathbf{H}\mathbf{D}\alpha\|_2^2 + \lambda \|\mathbf{w}\alpha\|_p, \quad (20)$$

where \mathbf{D} represents the dictionary and α is the sparse coefficient; \mathbf{w} is the weight in weighted ℓ_p -norm and λ is a regularization parameter.

A. ADMM based Algorithm for Weighted ℓ_p -norm Minimization

Solving the objective function of Eq. (20) is difficult, since it is a large scale non-convex optimization problem. In order to make the optimization tractable, we employ the alternating direction method of multipliers (ADMM) [58, 59], whose underlying principle is to split the unconstrained minimization problem into different constrained sub-problems. Numerical simulations have shown that ADMM can converge by only using a small memory footprint, which makes it attractive for various large-scale optimization problems [60–62].

Now, let us come back to Eq. (20) and use ADMM to solve it. We first turn Eq. (20) into another equivalent constrained form by introducing an auxiliary variable \mathbf{z} ,

$$\hat{\alpha} = \arg \min_{z, \alpha} \frac{1}{2} \|\mathbf{y} - \mathbf{H}\mathbf{z}\|_2^2 + \lambda \|\mathbf{w}\alpha\|_p, \text{ s.t. } \mathbf{z} = \mathbf{D}\alpha. \quad (21)$$

Following this, Eq. (21) can be transformed into three iterative steps:

$$\mathbf{z}^{t+1} = \arg \min_z \frac{1}{2} \|\mathbf{y} - \mathbf{H}\mathbf{z}\|_2^2 + \frac{\rho}{2} \|\mathbf{z} - \mathbf{D}\alpha^t - \mathbf{b}^t\|_2^2, \quad (22)$$

$$\alpha^{t+1} = \arg \min_{\alpha} \lambda \|\mathbf{w}\alpha\|_p + \frac{\rho}{2} \|\mathbf{z}^{t+1} - \mathbf{D}\alpha - \mathbf{b}^t\|_2^2, \quad (23)$$

$$\mathbf{b}^{t+1} = \mathbf{b}^t - (\mathbf{z}^{t+1} - \mathbf{D}\alpha^{t+1}). \quad (24)$$

One can observe that the minimization of Eq. (21) is separated into two minimization sub-problems, *i.e.*, \mathbf{z} and α sub-problem. Fortunately, there is an efficient solution to each sub-problem, which will be discussed in the following subsections. The superscript t is omitted for conciseness in the derivation below.

1) \mathbf{z} Sub-problem : Given α , \mathbf{z} sub-problem in Eq. (22) becomes

$$\min_z \mathcal{Q}_1(\mathbf{z}) = \min_z \frac{1}{2} \|\mathbf{y} - \mathbf{H}\mathbf{z}\|_2^2 + \frac{\rho}{2} \|\mathbf{z} - \mathbf{D}\alpha - \mathbf{b}\|_2^2. \quad (25)$$

This is a quadratic form and has a closed-form solution,

$$\hat{\mathbf{z}} = (\mathbf{H}^T\mathbf{H} + \rho\mathbf{I})^{-1} (\mathbf{H}^T\mathbf{y} + \rho(\mathbf{D}\alpha + \mathbf{b})), \quad (26)$$

where \mathbf{I} is an identity matrix with the desired dimension.

Owing to the specific structure of \mathbf{H} in image inpainting, Eq. (25) can be efficiently computed without matrix inversion. However, in image CS recovery, as \mathbf{H} is a random projection matrix, it is expensive to solve Eq. (26) directly. In this work, we employ the steepest descent method [63] to solve Eq. (25),

$$\hat{\mathbf{z}} = \mathbf{z} - \eta \mathbf{q}, \quad (27)$$

where \mathbf{q} is the gradient of the objective function $\mathcal{Q}_1(\mathbf{z})$, and η represents the step size.

Thereby, in image CS recovery, we only need an iterative calculation to solve \mathbf{z} sub-problem, *i.e.*,

$$\hat{\mathbf{z}} = \mathbf{z} - \eta (\mathbf{H}^T \mathbf{H} \mathbf{z} - \mathbf{H}^T \mathbf{y} + \rho(\mathbf{z} - \mathbf{D}\boldsymbol{\alpha} - \mathbf{b})), \quad (28)$$

where $\mathbf{H}^T \mathbf{H}$ and $\mathbf{H}^T \mathbf{y}$ can be pre-calculated.

2) $\boldsymbol{\alpha}$ Sub-problem: Given \mathbf{z} , $\boldsymbol{\alpha}$ sub-problem in Eq. (23) can be rewritten as

$$\min_{\boldsymbol{\alpha}} \mathcal{Q}_2(\boldsymbol{\alpha}) = \min_{\boldsymbol{\alpha}} \frac{1}{2} \|\mathbf{D}\boldsymbol{\alpha} - \mathbf{l}\|_2^2 + \frac{\lambda}{\rho} \|\mathbf{w}\boldsymbol{\alpha}\|_p, \quad (29)$$

where $\mathbf{l} = \mathbf{z} - \mathbf{b}$.

However, due to the complicated structure of $\|\mathbf{w}\boldsymbol{\alpha}\|_p$, it is challenging to solve Eq. (29) directly. Let $\mathbf{x} = \mathbf{D}\boldsymbol{\alpha}$, Eq. (29) can be rewritten as

$$\min_{\boldsymbol{\alpha}} \mathcal{Q}_2(\boldsymbol{\alpha}) = \min_{\boldsymbol{\alpha}} \frac{1}{2} \|\mathbf{x} - \mathbf{l}\|_2^2 + \frac{\lambda}{\rho} \|\mathbf{w}\boldsymbol{\alpha}\|_p. \quad (30)$$

Since the basic unit of the GSC model is patch group and in order to achieve a tractable solution to Eq. (30), a general assumption is made, and with which even a closed-form solution can be achieved. Specifically, \mathbf{l} can be regarded as a noisy observation of \mathbf{x} , and then the assumption is made that each element of $\mathbf{e} = \mathbf{x} - \mathbf{l}$ follows an independent zero-mean Gaussian distribution with variance σ_n^2 . Provided this assumption, we have the following theorem.

Theorem 3. Define $\mathbf{x}, \mathbf{l} \in \mathbb{R}^N$, $\mathbf{X}_i, \mathbf{L}_i \in \mathbb{R}^{d \times m}$, and e_j denotes the j -th element of the error vector $\mathbf{e} \in \mathbb{R}^N$, where $\mathbf{e} = \mathbf{x} - \mathbf{l}$. Assume that e_j follows an independent zero mean Gaussian distribution with variance σ_n^2 , and thus for any $\xi > 0$, we can represent the relationship between $\frac{1}{N} \|\mathbf{x} - \mathbf{l}\|_2^2$ and $\frac{1}{S} \sum_{i=1}^n \|\mathbf{X}_i - \mathbf{L}_i\|_F^2$ by the following property,

$$\lim_{\substack{N \rightarrow \infty \\ S \rightarrow \infty}} \mathbf{P} \left(\left| \frac{1}{N} \|\mathbf{x} - \mathbf{l}\|_2^2 - \frac{1}{S} \sum_{i=1}^n \|\mathbf{X}_i - \mathbf{L}_i\|_F^2 \right| < \xi \right) = 1, \quad (31)$$

where $\mathbf{P}(\cdot)$ represents the probability and $S = d \times m \times n$.

Proof. See [5]. \square

Then, based on Theorem 3, we have the following equation with a very large probability (limited to 1) at each iteration,

$$\frac{1}{N} \|\mathbf{x} - \mathbf{l}\|_2^2 = \frac{1}{S} \sum_{i=1}^n \|\mathbf{X}_i - \mathbf{L}_i\|_F^2. \quad (32)$$

Therefore, Based on Eqs. (30) and (32), we have

$$\begin{aligned} & \min_{\boldsymbol{\alpha}} \frac{1}{2} \|\mathbf{x} - \mathbf{l}\|_2^2 + \frac{\lambda}{\rho} \|\mathbf{w}\boldsymbol{\alpha}\|_p \\ &= \min_{\{\mathbf{A}_i\}_{i=1}^n} \sum_{i=1}^n \left(\frac{1}{2} \|\mathbf{X}_i - \mathbf{L}_i\|_F^2 + \tau \|\mathbf{W}_i \circ \mathbf{A}_i\|_p \right) \\ &= \min_{\{\mathbf{A}_i\}_{i=1}^n} \sum_{i=1}^n \left(\frac{1}{2} \|\mathbf{L}_i - \mathbf{D}_i \mathbf{A}_i\|_F^2 + \tau \|\mathbf{W}_i \circ \mathbf{A}_i\|_p \right), \end{aligned} \quad (33)$$

Algorithm 1 ADMM for weighted ℓ_p -norm minimization.

Require: The observed image \mathbf{y} and the measurement matrix

- \mathbf{H} .
- 1: Set parameters $t, \mathbf{b}, \mathbf{z}, \boldsymbol{\alpha}, C, d, m, \rho, p, \sigma_n, \epsilon$ and ε .
 - 2: **for** $t = 0$ **to** Max-Iter **do**
 - 3: **if** \mathbf{H} is mask operator **then**
 - 4: Update \mathbf{z}^{t+1} by Eq. (26);
 - 5: **else if** \mathbf{H} is random projection operator **then**
 - 6: Update \mathbf{z}^{t+1} by Eq. (28);
 - 7: **end if**
 - 8: $\mathbf{l}^{t+1} = \mathbf{z}^{t+1} - \mathbf{b}^t$;
 - 9: **for** Each group \mathbf{L}_i **do**
 - 10: Construct dictionary \mathbf{D}_i by computing Eq. (10);
 - 11: Update λ^{t+1} by computing Eq. (37);
 - 12: Update τ^{t+1} by computing $\tau = \frac{\lambda S}{\rho N}$;
 - 13: Update \mathbf{w}_i^{t+1} by computing Eq. (36);
 - 14: Update $\boldsymbol{\alpha}_i^{t+1}$ by computing Eq. (35);
 - 15: **end for**
 - 16: Update \mathbf{D}^{t+1} by concatenating all \mathbf{D}_i .
 - 17: Update $\boldsymbol{\alpha}^{t+1}$ by concatenating all $\boldsymbol{\alpha}_i$.
 - 18: Update \mathbf{b}^{t+1} by computing Eq. (24).
 - 19: **end for**
 - 20: **Output:** The final restored image $\hat{\mathbf{x}} = \mathbf{D}\boldsymbol{\alpha}$.

where \circ represents the element-wise product of two matrices (Hadamard product); $\mathbf{X}_i = \mathbf{D}_i \mathbf{A}_i$ and $\tau = \frac{\lambda S}{\rho N}$. Clearly, Eq. (33) can be viewed as the GSC problem by solving n sub-problems for each patch group \mathbf{X}_i [5–8]. \mathbf{A}_i represents the group sparse coefficient of each patch group \mathbf{X}_i , and \mathbf{W}_i is a weight assigned to each patch group \mathbf{X}_i . Each weight matrix \mathbf{W}_i will enhance the representation capability of each group sparse coefficient \mathbf{A}_i . Note that here we abuse the p -norm for matrix and the ℓ_p -norm is imposed on each column of group sparse coefficient \mathbf{A}_i . Based on Lemma 2, Eq. (33) can be rewritten as

$$\begin{aligned} \{\hat{\mathbf{A}}_i\}_{i=1}^n &= \min_{\{\mathbf{A}_i\}_{i=1}^n} \sum_{i=1}^n \left(\frac{1}{2} \|\mathbf{R}_i - \mathbf{A}_i\|_F^2 + \tau \|\mathbf{W}_i \circ \mathbf{A}_i\|_p \right) \\ &= \min_{\{\boldsymbol{\alpha}_i\}_{i=1}^n} \sum_{i=1}^n \left(\frac{1}{2} \|\boldsymbol{\gamma}_i - \boldsymbol{\alpha}_i\|_2^2 + \tau \|\mathbf{w}_i \boldsymbol{\alpha}_i\|_p \right), \end{aligned} \quad (34)$$

where $\mathbf{L}_i = \mathbf{D}_i \mathbf{R}_i$; $\boldsymbol{\alpha}_i, \boldsymbol{\gamma}_i$ and \mathbf{w}_i denote the vectorization of the matrix $\mathbf{A}_i, \mathbf{R}_i$ and \mathbf{W}_i , respectively.

Therefore, the minimization problem of Eq. (29) can be simplified to solve the minimization problem in Eq. (34). To obtain the solution of Eq. (34) effectively, we develop a generalized soft-thresholding (GST) algorithm [64] to solve it. Specifically, a closed-form solution of Eq. (34) can be computed by

$$\boldsymbol{\alpha}_i = \text{GST}(\boldsymbol{\gamma}_i, \tau \mathbf{w}_i, p). \quad (35)$$

Please refer to [64] for more details about the GST algorithm.

B. Setting the Weight and Regularization Parameter

As large values in coefficient $\boldsymbol{\alpha}_i$ usually depict major edge and texture information [16], in order to reconstruct \mathbf{X}_i from its



Fig. 3. Test images. Top row, from left to right: Mickey, Barbara, Butterfly, Elaine, Fence, Straw, Mural, Peppers. Bottom row, from left to right: House, Starfish, Fence, Nanna, Lena, Fireman, Bridge, Zebra.

degraded one, we usually shrink the larger values less, while shrinking smaller ones more [25]. Therefore, we let

$$w_i = \frac{1}{|\gamma_i| + \epsilon}, \quad (36)$$

with ϵ as a small positive constant.

The regularization parameter λ that balances the fidelity term and the regularization term should be adaptively determined for better reconstruction performance. Inspired by [65], λ of each patch group L_i in each iteration is set to:

$$\lambda = \frac{2\sqrt{2}\sigma_n^2}{\varphi_i + \epsilon}. \quad (37)$$

where φ_i denotes the estimated variance of γ_i , and ϵ is a small positive constant.

After solving the two sub-problems, we summarize the entire algorithm for Eq. (20) in Algorithm 1.

V. EXPERIMENTAL RESULTS

In this section, extensive experiments are presented to validate the feasibility of the proposed benchmark, *i.e.*, demonstrate that the results of the weighted ℓ_p -norm ($w\ell_p$ -norm) minimization in sparse coding are consistent with the ones of our previous analysis (WSNM) in Section III-C. We compare the $w\ell_p$ -norm minimization with the other three well-known norm minimization methods based on the GSC framework, including ℓ_1 -norm minimization, weighted ℓ_1 -norm ($w\ell_1$ -norm) minimization and the ℓ_p -norm minimization. We conduct the performance evaluations on image inpainting and image CS recovery. The peak signal-to-noise ratio (PSNR) metric is adopted to evaluate the quality of the restored images. We have also calculated the full reference image quality assessment (FR-IQA) metrics [66, 67] of the restored images, *i.e.*, FSIM [66], which shows similar results to PSNR and thus omitted here due to the limited space. The experimental test images are shown in Fig. 3. Due to limited space, please enlarge the tables and figures on the screen for better comparison. The source code of the proposed method is available at: <https://drive.google.com/open?id=1J3cgJF2zrvyL08COy4eexwNk-wErUv1>.

A. Parameter Selection

The parameters used in the algorithm are empirically chosen according to different applications in order to achieve relatively good results. Note that all norm minimization methods are based on the designed adaptive dictionary learning (ADL) scheme under the GSC framework.

TABLE I
DETAILED SETTING OF ρ, λ FOR IMAGE INPAINTING AND IMAGE CS RECOVERY WITH THE DESIGNED ADAPTIVE DICTIONARY LEARNING APPROACH.

Image Inpainting						
ADL	ℓ_1 -norm		ℓ_p -norm		$w\ell_1$ -norm	$w\ell_p$ -norm
Parameters	ρ	λ	ρ	λ	ρ	ρ
80%	7e-5	5e-6	0.006	0.07	0.1	0.0003
70%	1e-4	7e-6	0.008	0.07	0.1	0.0003
60%	1e-5	1e-6	7e-5	3e-6	0.1	0.03
50%	5e-5	1e-5	0.0001	7e-6	0.1	0.04
Image CS Recovery						
ADL	ℓ_1 -norm		ℓ_p -norm		$w\ell_1$ -norm	$w\ell_p$ -norm
Parameters	ρ	λ	ρ	λ	ρ	ρ
0.2N	0.001	5e-5	0.003	5e-4	0.1	0.0005
0.3N	0.003	7e-4	0.01	3e-4	0.1	0.05
0.4N	0.003	5e-4	0.006	3e-4	0.1	0.05
0.5N	0.003	5e-4	0.006	3e-4	0.2	0.05

In image inpainting, the mask is generated randomly. The size of patch is set to 8×8 . The similar patch number m is set to 60. The searching window $C \times C$ is set to 25×25 ; $\sigma_n = \sqrt{2}$; p is set to 0.45, 0.45, 0.95 and 0.95 when 80%, 70%, 60% and 50% pixels are missing, respectively. ϵ and ϵ are set as (0.35, 0.35) and (0.1, 0.3) for $w\ell_1$ -norm and $w\ell_p$ -norm, respectively. The detailed settings of ρ and λ are shown on the upper part of Table I. Due to the existence of the weight w , λ is computed by Eq. (37) in $w\ell_1$ -norm and $w\ell_p$ -norm. We will give a detailed discussion on how to choose the best power p in Sec. V-D.

In image CS recovery, we generate the CS measurements at the block level by utilizing a Gaussian random projection matrix to test images, *i.e.*, CS with block size 32×32 [44]. The patch size is set to 7×7 . The similar patch number $m = 60$, and the search window $C \times C$ is set to 20×20 ; $\sigma_n = \sqrt{2}$; p is set to 0.5, 0.95, 0.95 and 0.95 with 0.2N, 0.3N, 0.4N and 0.5N measurements, respectively. ϵ and ϵ are set as (0.35, 0.35) and (0.1, 0.4) for $w\ell_1$ -norm and $w\ell_p$ -norm, respectively. Similarly, λ is computed by Eq. (37) in $w\ell_1$ -norm and $w\ell_p$ -norm. The detailed settings of ρ and λ are shown at the lower part of Table I.

In addition, to make a fair comparison of all norm minimization methods, the iterative stopping criterion is set to: $\text{PSNR}(t+1) - \text{PSNR}(t) < 0$, where $\text{PSNR}(t+1)$ and $\text{PSNR}(t)$ denote the PSNR values of the restored images at the $(t+1)$ -th iteration and t -th iteration, respectively.

B. Comparisons of ℓ_1 -norm, Weighted ℓ_1 -norm, ℓ_p -norm and Weighted ℓ_p -norm

We first compare four norm minimization methods, *i.e.*, ℓ_1 -norm minimization, $w\ell_1$ -norm minimization, ℓ_p -norm minimization and the $w\ell_p$ -norm minimization, based on the designed ADL scheme for image inpainting and image CS recovery.

The PSNR results of image inpainting and image CS recovery are shown in Table II and Table III, respectively. It can be seen that the $w\ell_p$ -norm minimization achieves better results than the other three norm minimization methods in most cases in terms of PSNR. Fig. 4 shows the image inpainting results of image *Mickey* with 80% pixels missing. Fig. 5 displays the image CS recovery results of image *Straw* with 0.2N measurements. We can observe that the $w\ell_p$ -norm minimization

TABLE II
PSNR (dB) COMPARISON OF ℓ_1 -NORM, ℓ_p -NORM, $w\ell_1$ -NORM AND THE $w\ell_p$ -NORM, BASED ON THE DESIGNED ADL METHOD FOR IMAGE INPAINTING.

Miss pixels	Methods	Mickey	Butterfly	Fence	Starfish	Nanna	Zebra	Fireman	Mural	Average
80%	ℓ_1 -norm	25.97	25.61	28.90	26.98	25.46	22.33	25.39	25.29	25.74
	ℓ_p -norm	26.74	26.36	29.47	27.54	25.87	23.05	25.63	25.69	26.29
	$w\ell_1$ -norm	26.66	26.39	29.98	28.00	25.73	22.39	25.68	26.12	26.37
	$w\ell_p$ -norm	26.92	26.52	30.00	28.05	25.95	23.06	25.80	26.26	26.57
70%	ℓ_1 -norm	27.86	27.86	30.72	29.02	27.32	24.26	27.05	27.40	27.69
	ℓ_p -norm	29.04	29.10	31.54	30.25	28.31	25.19	27.69	28.37	28.69
	$w\ell_1$ -norm	29.16	29.21	31.83	30.54	28.07	24.82	27.81	28.53	28.74
	$w\ell_p$ -norm	29.29	29.28	31.85	30.56	28.39	25.13	27.84	28.62	28.87
60%	ℓ_1 -norm	29.61	29.82	32.29	30.78	29.02	25.93	28.53	28.93	29.36
	ℓ_p -norm	29.85	30.16	32.51	31.14	29.22	26.13	28.69	29.16	29.61
	$w\ell_1$ -norm	31.44	31.40	33.65	32.93	30.42	27.04	29.74	30.27	30.86
	$w\ell_p$ -norm	31.46	31.54	33.67	33.02	30.56	27.21	29.77	30.35	30.95
50%	ℓ_1 -norm	31.62	31.46	33.78	32.62	30.68	27.65	30.13	30.48	31.05
	ℓ_p -norm	31.88	31.78	33.97	32.99	30.89	27.86	30.28	30.70	31.29
	$w\ell_1$ -norm	33.98	33.16	35.30	34.99	32.38	29.12	31.31	31.88	32.76
	$w\ell_p$ -norm	34.01	33.26	35.25	35.05	32.53	29.26	31.32	31.91	32.82

TABLE III
PSNR (dB) COMPARISON OF ℓ_1 -NORM, ℓ_p -NORM, $w\ell_1$ -NORM AND THE $w\ell_p$ -NORM, BASED ON THE DESIGNED ADL METHOD FOR IMAGE CS RECOVERY.

Ratio	Methods	Barbara	Bridge	Elaine	Fence	House	Lena	Peppers	Straw	Average
0.2	ℓ_1 -norm	32.24	25.03	34.59	29.31	36.01	30.77	30.00	24.11	30.26
	ℓ_p -norm	34.31	25.13	35.75	29.99	37.15	31.50	30.79	24.82	31.18
	$w\ell_1$ -norm	34.53	25.04	36.22	30.19	37.07	31.49	31.22	24.82	31.32
	$w\ell_p$ -norm	34.55	25.28	36.00	30.38	36.92	31.62	31.32	25.06	31.39
0.3	ℓ_1 -norm	34.49	26.49	36.76	31.16	37.94	32.97	31.93	26.11	32.23
	ℓ_p -norm	34.86	26.59	37.07	31.42	38.29	33.15	32.22	26.23	32.48
	$w\ell_1$ -norm	37.10	27.25	38.26	32.50	39.07	34.26	33.39	27.84	33.71
	$w\ell_p$ -norm	37.23	27.22	38.30	32.53	39.23	34.29	33.32	27.89	33.75
0.4	ℓ_1 -norm	36.79	27.94	38.58	32.84	39.70	34.76	33.63	27.95	34.03
	ℓ_p -norm	37.15	28.06	38.87	33.09	39.98	34.95	33.91	28.10	34.26
	$w\ell_1$ -norm	39.04	28.90	40.03	34.50	40.82	36.58	35.10	30.30	35.66
	$w\ell_p$ -norm	39.13	28.85	40.05	34.42	40.93	36.66	35.00	30.28	35.67
0.5	ℓ_1 -norm	38.80	29.38	40.26	34.50	41.27	36.56	35.18	29.88	35.73
	ℓ_p -norm	39.19	29.51	40.54	34.75	41.52	36.78	35.43	30.07	35.97
	$w\ell_1$ -norm	40.84	30.51	41.52	36.29	42.25	38.99	36.56	32.49	37.43
	$w\ell_p$ -norm	40.94	30.52	41.63	36.24	42.38	39.09	36.53	32.46	37.47

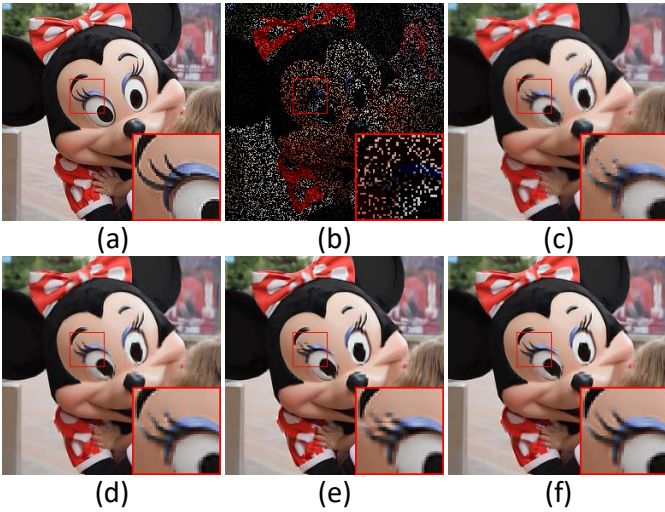


Fig. 4. Inpainting performance comparison of Mickey based on the *designed adaptive dictionary learning* method. (a) Original image; (b) Degraded image with 80% pixels missing; (c) ℓ_1 -norm (PSNR= 25.97dB); (d) ℓ_p -norm (PSNR= 26.74dB); (e) $w\ell_1$ -norm (PSNR= 26.66dB); (f) $w\ell_p$ -norm (PSNR= 26.92dB).

obtains better perceptual quality than the other three norm minimization methods. Therefore, these experimental results are consistent with our previous analysis. This demonstrates the proposed benchmark is feasible.

Next, in order to further prove the universality and advantage of the proposed scheme, instead of using the designed ADL method, we exploit another two generalized dictionary

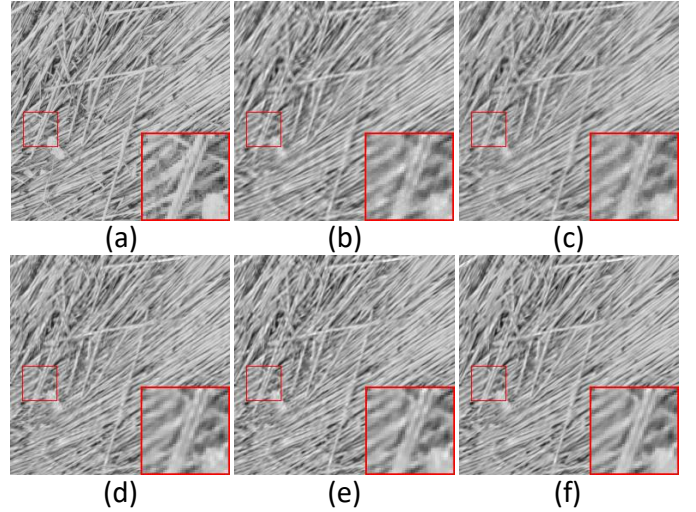


Fig. 5. CS recovery performance comparison of *Straw* with $0.2N$ measurements based on the *designed adaptive dictionary learning* method. (a) Original image; (b) Initial recovered image by [44] (PSNR= 23.76dB); (c) ℓ_1 -norm (PSNR= 24.11dB); (d) ℓ_p -norm (PSNR= 24.82dB); (e) $w\ell_1$ -norm (PSNR= 24.82dB); (f) $w\ell_p$ -norm (PSNR= 25.06dB).

TABLE IV
DETAILED SETTING OF ρ , λ FOR IMAGE INPAINTING AND IMAGE CS RECOVERY, WITH THE GRAPH-BASED DICTIONARY [42] AND PCA DICTIONARY [43].

Image Inpainting						
Graph	ℓ_1 -norm		ℓ_p -norm		$w\ell_1$ -norm	$w\ell_p$ -norm
Parameters	ρ	λ	ρ	λ	ρ	ρ
80%	0.008	1e-5	0.003	7e-5	0.15	0.06
70%	0.003	1e-5	0.003	7e-5	0.1	0.05
60%	0.006	7e-5	0.003	5e-5	0.07	0.09
50%	0.003	7e-5	0.003	9e-5	0.05	0.05
Image CS Recovery						
PCA	ℓ_1 -norm		ℓ_p -norm		$w\ell_1$ -norm	$w\ell_p$ -norm
Parameters	ρ	λ	ρ	λ	ρ	ρ
0.2N	0.03	1e-6	0.003	7e-5	0.09	0.07
0.3N	0.008	1e-6	0.006	7e-5	0.07	0.09
0.4N	0.008	1e-6	0.008	1e-5	0.05	0.05
0.5N	0.008	1e-6	0.008	1e-5	0.05	0.05

learning methods to verify the feasibility of the proposed benchmark, *i.e.*, graph-based dictionary learning method [42] and PCA dictionary learning method [43] for image inpainting and image CS recovery, respectively. Similar to the designed ADL method, we learn the graph-based dictionary and the PCA dictionary from each patch group of the degraded image. All the parameters remain the same as specified in the subsection V-A except for ρ and λ , which are now shown in Table IV. The PSNR comparison results for image inpainting of four competing methods are shown in Table V. It can be seen that the $w\ell_p$ -norm minimization consistently outperforms the other three norm minimization methods for all test images (the only exception is the image *Zebra* for which the $w\ell_1$ -norm minimization is slightly higher than the $w\ell_p$ -norm minimization in the scene of 80% and 70% pixels missing). The PSNR comparison results for image CS recovery are shown in Table VI, and we can observe that the $w\ell_p$ -norm minimization outperforms the other three norm minimization methods in most cases. Fig. 6 shows the visual comparison of image *Fence* with 80% pixels missing for image inpainting based on the graph-based dictionary learning method. The visual comparison of image *Peppers* with $0.2N$ measurements

TABLE V

PSNR (dB) COMPARISON OF ℓ_1 -NORM, ℓ_p -NORM, $w\ell_1$ -NORM AND THE $w\ell_p$ -NORM, BASED ON THE GRAPH-BASED DICTIONARY LEARNING METHOD [42] FOR IMAGE INPAINTING.

Miss pixels	Methods	Mickey	Butterfly	Fence	Starfish	Nanna	Zebra	Fireman	Mural	Average
80%	ℓ_1 -norm	24.63	23.62	22.92	26.27	25.52	20.45	24.59	23.57	23.82
	ℓ_p -norm	25.20	24.51	25.83	26.41	24.79	20.79	24.88	24.31	24.59
	$w\ell_1$ -norm	25.30	24.63	26.67	26.20	24.75	20.98	24.88	24.44	24.73
	$w\ell_p$ -norm	25.40	24.74	26.99	26.43	24.92	20.97	25.00	24.60	24.88
70%	ℓ_1 -norm	26.31	25.75	25.06	28.07	26.21	21.84	26.08	25.33	25.58
	ℓ_p -norm	27.21	26.88	28.27	28.33	26.58	22.43	26.50	26.43	26.58
	$w\ell_1$ -norm	27.37	27.00	28.89	27.92	26.58	22.80	26.55	26.65	26.72
	$w\ell_p$ -norm	27.49	27.19	29.12	28.50	26.81	22.77	26.77	26.84	26.93
60%	ℓ_1 -norm	27.58	27.50	27.48	29.46	27.61	23.37	27.38	26.80	27.15
	ℓ_p -norm	27.72	27.66	28.09	29.47	27.65	23.46	27.41	26.93	27.30
	$w\ell_1$ -norm	28.79	28.84	30.74	29.68	28.22	24.72	28.05	28.39	28.43
	$w\ell_p$ -norm	28.80	28.91	30.79	29.81	28.29	24.75	28.11	28.45	28.49
50%	ℓ_1 -norm	29.14	29.24	29.73	30.93	29.13	24.84	28.78	28.37	28.77
	ℓ_p -norm	29.31	29.40	30.24	30.86	29.12	24.98	28.80	28.50	28.90
	$w\ell_1$ -norm	30.68	30.62	32.65	31.51	29.76	26.61	29.64	30.04	30.19
	$w\ell_p$ -norm	30.71	30.69	32.71	31.56	29.82	26.62	29.70	30.08	30.24

TABLE VI

PSNR (dB) COMPARISON OF ℓ_1 -NORM, ℓ_p -NORM, $w\ell_1$ -NORM AND THE $w\ell_p$ -NORM, BASED ON THE PCA DICTIONARY LEARNING METHOD [43] FOR IMAGE CS RECOVERY.

Ratio	Methods	Barbara	Bridge	Elaine	Fence	House	Lena	Peppers	Straw	Average
0.2	ℓ_1 -norm	32.13	25.05	34.60	29.12	35.92	30.78	30.08	24.10	30.22
	ℓ_p -norm	34.07	25.24	35.74	29.87	36.76	31.46	30.87	24.74	31.09
	$w\ell_1$ -norm	32.89	25.25	33.32	29.87	36.23	31.23	31.10	24.50	30.55
	$w\ell_p$ -norm	34.09	25.29	35.74	30.14	36.75	31.48	31.31	24.89	31.21
0.3	ℓ_1 -norm	34.38	26.53	36.80	31.08	38.05	33.03	32.10	26.09	32.26
	ℓ_p -norm	34.50	26.59	36.84	31.19	38.04	33.09	32.24	26.18	32.33
	$w\ell_1$ -norm	35.53	26.95	34.94	31.73	38.04	33.69	32.99	27.05	32.61
	$w\ell_p$ -norm	35.69	27.04	37.25	31.84	38.07	33.80	33.06	27.28	33.01
0.4	ℓ_1 -norm	36.69	28.01	38.65	32.84	39.80	34.83	33.85	27.96	34.08
	ℓ_p -norm	37.03	28.13	38.92	33.09	40.07	35.04	34.10	28.10	34.31
	$w\ell_1$ -norm	37.63	28.39	39.03	33.43	39.75	35.46	34.59	29.07	34.67
	$w\ell_p$ -norm	37.74	28.45	39.11	33.51	39.84	35.57	34.65	29.21	34.76
0.5	ℓ_1 -norm	38.72	29.46	40.32	34.55	41.36	36.64	35.45	29.89	35.80
	ℓ_p -norm	39.09	29.60	40.59	34.80	41.59	36.88	35.66	30.07	36.03
	$w\ell_1$ -norm	39.53	29.95	40.59	35.13	41.25	37.45	36.09	31.16	36.39
	$w\ell_p$ -norm	39.64	30.00	40.67	35.21	41.33	37.56	36.14	31.30	36.48

for image CS recovery based on the PCA dictionary learning method is shown in Fig. 7. It can be observed that the $w\ell_p$ -norm minimization achieves better visual quality than the other three norm minimization methods. This again verifies the feasibility of the proposed benchmark.

We also notice that for various dictionary learning methods, the results of the $w\ell_p$ -norm minimization are usually a little bit (~ 0.1 dB) better than those of the $w\ell_1$ -norm minimization, which is consistent with the observation in [26]. Comparing Tables II-III with Tables V-VI, we can see that the designed ADL method can provide better performance than the graph-based dictionary learning and PCA dictionary learning methods. This demonstrates the superiority of the designed adaptive dictionary learning method, while further illustrating the feasibility of the proposed benchmark in sparse coding.

C. Comparison with Other Leading Algorithms

We now validate the performance of the proposed scheme, *i.e.*, group-based sparse coding with non-convex $w\ell_p$ -norm (GSC- $w\ell_p$) minimization for image inpainting and image CS recovery with the designed adaptive dictionary learning method, through comparing it with recent state-of-the-art methods⁵.

In image inpainting, we compare the proposed GSC- $w\ell_p$ with nine state-of-the-art methods: SALSA [47], BPFA [48],

⁵We would like to thank the authors of [44, 47–56, 68–72] for kindly providing their software or codes.

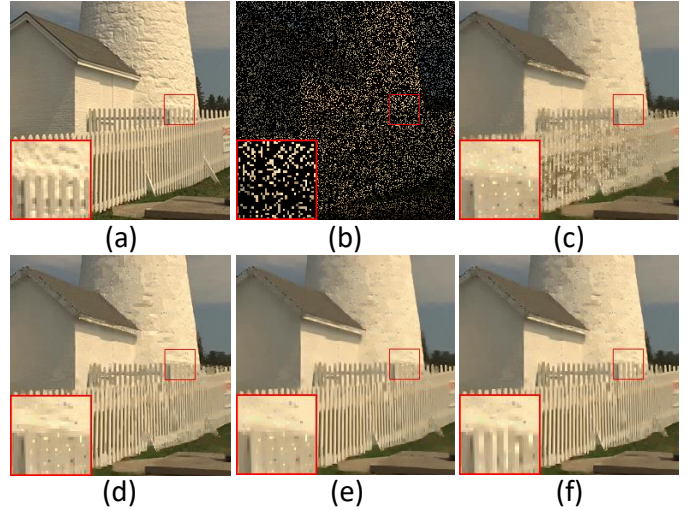


Fig. 6. Inpainting performance comparison on the image *Fence* based on the *graph-based dictionary learning* method [42]. (a) Original image; (b) Degraded image with 80% missing sample; (c) ℓ_1 -norm (PSNR=22.92dB); (d) ℓ_p -norm (PSNR=25.83dB); (e) $w\ell_1$ -norm (PSNR=26.67dB); (f) $w\ell_p$ -norm (PSNR=26.99dB).

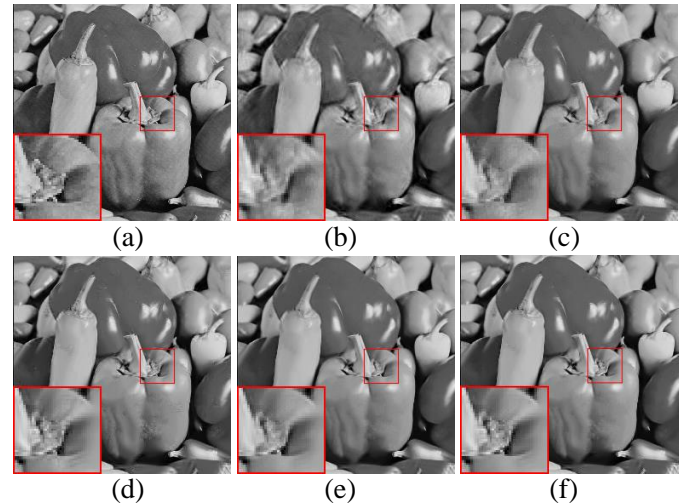


Fig. 7. CS recovery performance comparison with $0.2N$ measurements on the image *Peppers* based on the *PCA dictionary learning* method [43]. (a) Original image; (b) Initial image by [44] (PSNR=28.61dB); (c) ℓ_1 -norm (PSNR=30.08dB); (d) ℓ_p -norm (PSNR=30.87dB); (e) $w\ell_1$ -norm (PSNR=31.10dB); (f) $w\ell_p$ -norm (PSNR=31.31dB).

IPPO [49], JSM [50], Aloha [51], BKSVD [68], NGS [69], IRCNN [71] and IDBP [72]. Note that BPFA, IPPO, JSM and Aloha are the image inpainting baseline methods. IRCNN and IDBP are the deep learning based methods, which use strong deep convolutional neural network (CNN) priors. Table VII lists the PSNR results for a collection of 8 color images for these methods. It can be seen that the proposed GSC- $w\ell_p$ outperforms the other competing methods in most cases. The average gains of the proposed GSC- $w\ell_p$ over SALSA, BPFA, IPPO, JSM, Aloha, BKSVD, NGS, IRCNN and IDBP methods are as much as 4.06dB, 2.26dB, 1.06dB, 1.25dB, 1.62dB, 2.93dB, 2.70dB, 0.43dB and 1.21dB, respectively. The visual comparisons of image *Zebra* and image *Starfish* with 80% pixels missing are shown in Fig. 8 and Fig. 9, respectively. It can be seen that SALSA and BKSVD could not reconstruct sharp edges and fine details. The BPFA, IPPO, JSM, Aloha,

TABLE VII
PSNR (dB) COMPARISON OF SALSA [47], BPFA [48], IPPO [49], JSM [50], ALOHA [51], BKSVD [68], NGS [69], IRCNN [71], IDBP [72] AND GSC- wl_p FOR IMAGE INPAINTING.

Miss pixels	Methods	Mickey	Butterfly	Fence	Starfish	Nanna	Zebra	Fireman	Mural	Average
80%	SALSA	24.46	22.85	21.80	25.70	24.12	19.68	24.38	23.15	23.27
	BPFA	24.53	24.04	26.24	26.79	24.71	20.90	24.88	24.13	24.53
	IPPO	26.33	25.13	27.98	26.30	25.60	22.71	25.56	25.66	25.66
	JSM	26.09	25.57	28.59	27.07	25.33	21.88	25.31	25.40	25.65
	Aloha	25.33	24.88	28.88	26.33	25.54	22.72	25.03	25.23	25.49
	BKSVD	23.72	22.00	24.20	25.36	23.97	19.37	23.79	23.02	23.18
	NGS	24.50	23.85	25.26	26.17	24.58	20.49	24.54	23.78	24.15
	IRCNN	26.45	25.34	27.76	27.01	25.76	22.43	25.78	25.75	25.78
	IDBP	25.40	25.24	25.03	26.88	25.51	20.97	25.42	25.26	24.96
GSC- wl_p	26.92	26.52	30.00	28.05	25.95	23.06	25.80	26.26	26.57	
70%	SALSA	25.98	25.06	23.57	27.55	25.44	21.41	25.82	25.00	24.98
	BPFA	26.16	26.68	28.87	28.93	26.62	22.78	26.55	26.46	26.63
	IPPO	28.59	27.68	30.08	28.91	27.44	24.76	27.44	27.92	27.85
	JSM	28.25	27.97	30.46	29.36	27.34	23.95	27.16	27.59	27.76
	Aloha	27.11	27.29	30.57	28.22	27.43	24.55	26.52	27.33	27.38
	BKSVD	26.17	25.00	28.35	27.79	26.18	23.06	25.85	25.57	26.00
	NGS	26.68	26.36	27.32	28.35	26.35	22.71	26.29	26.06	26.27
	IRCNN	29.65	28.33	30.53	29.78	28.27	25.04	27.87	28.72	28.53
	IDBP	28.69	28.29	29.24	29.28	27.24	23.60	27.63	27.68	27.71
GSC- wl_p	29.29	29.28	31.85	30.56	28.39	25.13	27.84	28.61	28.87	
60%	SALSA	27.41	26.79	25.45	29.09	26.94	22.80	27.15	26.66	26.54
	BPFA	27.83	28.88	30.79	30.98	28.63	24.53	28.23	28.30	28.52
	IPPO	30.76	29.85	32.14	31.09	29.41	26.79	29.13	29.57	29.84
	JSM	29.85	29.83	32.23	31.40	29.09	25.90	28.79	29.24	29.54
	Aloha	28.59	29.16	32.33	30.19	29.51	26.24	28.24	28.92	29.15
	BKSVD	28.53	27.70	30.72	29.99	28.35	25.27	27.97	27.90	28.30
	NGS	28.09	28.37	30.11	30.26	28.06	24.39	27.67	27.99	28.12
	IRCNN	31.81	30.41	32.45	32.28	30.48	27.03	29.85	30.57	30.61
	IDBP	31.18	30.03	31.25	31.79	29.51	25.97	29.28	29.79	29.85
GSC- wl_p	31.46	31.54	33.67	33.02	30.56	27.21	29.77	30.35	30.95	
50%	SALSA	28.98	28.52	27.25	30.90	28.53	24.42	28.54	28.20	28.17
	BPFA	29.43	30.98	32.82	33.13	30.68	26.37	30.12	30.46	30.50
	IPPO	32.74	31.69	33.95	33.10	31.17	28.42	30.82	31.11	31.63
	JSM	31.96	31.47	33.75	33.24	30.75	27.77	30.37	30.89	31.27
	Aloha	30.33	30.78	33.79	31.85	31.24	27.67	29.88	30.28	30.73
	BKSVD	29.95	29.64	32.44	31.99	30.15	26.97	29.47	29.59	30.02
	NGS	29.75	30.28	32.00	32.10	29.71	26.03	29.22	29.88	29.87
	IRCNN	34.22	32.47	34.30	34.47	32.41	29.17	31.45	32.19	32.59
	IDBP	33.14	32.44	33.24	33.81	31.35	28.65	30.97	31.35	31.87
GSC- wl_p	34.00	33.26	35.25	35.05	32.53	29.26	31.32	31.91	32.82	

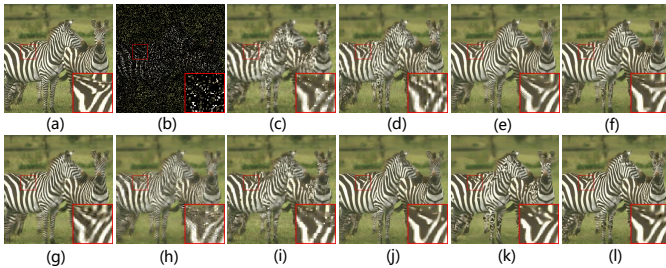


Fig. 8. Inpainting performance comparison on the image *Zebra*. (a) Original image; (b) Degraded image with 80% pixels missing sample; (c) SALSA [47] (PSNR = 19.68dB); (d) BPFA [48] (PSNR = 20.90dB); (e) IPPO [49] (PSNR = 22.71dB); (f) JSM [50] (PSNR = 21.88dB); (g) Aloha [51] (PSNR = 22.72dB); (h) BKSVD [68] (PSNR = 19.37dB); (i) NGS [69] (PSNR = 20.49dB); (j) IRCNN [71] (PSNR = 22.43dB); (k) IDBP [72] (PSNR = 20.97dB); (l) GSC- wl_p (PSNR = **23.06dB**).

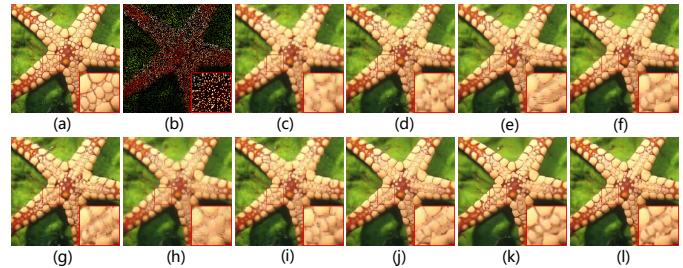


Fig. 9. Inpainting performance comparison on the image *Starfish*. (a) Original image; (b) Degraded image with 80% pixels missing sample; (c) SALSA [47] (PSNR = 25.70dB); (d) BPFA [48] (PSNR = 26.79dB); (e) IPPO [49] (PSNR = 26.30dB); (f) JSM [50] (PSNR = 27.07dB); (g) Aloha [51] (PSNR = 26.33dB); (h) BKSVD [68] (PSNR = 25.36dB); (i) NGS [69] (PSNR = 26.17dB); (j) IRCNN [71] (PSNR = 27.01dB); (k) IDBP [72] (PSNR = 26.88dB); (l) GSC- wl_p (PSNR = **28.05dB**).

NGS, IRCNN and IDBP methods produce the restored images with a much better visual quality than SALSA and BKSVD, but still suffer from some undesirable artifacts, such as the ringing effects. The proposed GSC- wl_p not only preserves sharp edges and fine details, but also eliminates the ringing effects.

In image CS recovery, we compare the proposed GSC- wl_p with eight competitive methods including BCS [44], RCOS [52], ASNR [53], ALSB [54], SGR [55], JASR [56],

NGS [69] and PMDSE [70]. Note that JASR is a recently block-based image CS recovery method that delivers state-of-the-art reconstruction results. The PSNR results are shown in Table VIII. One can observe that the proposed GSC- wl_p consistently outperforms the other competing methods in terms of PSNR (the only exception is the image *House* with 0.2N measurements for which ASNR slightly outperforms the proposed GSC- wl_p). The proposed GSC- wl_p achieves 6.08dB, 2.61dB, 0.36dB, 1.33dB, 1.01dB, 0.65dB, 3.45dB and

TABLE VIII
PSNR (dB) COMPARISON OF BCS [44], RCOS [52], ASNR [53], ALSB [54], SGSR [55], JASR [56], NGS [69], PMDSE [70] AND GSC- wl_p FOR IMAGE CS RECOVERY.

Ratio	Methods	Barbara	Bridge	Elaine	Fence	House	Lena	Peppers	Straw	Average
0.2	BCS	24.24	23.61	31.18	21.57	30.54	28.15	27.15	20.69	25.89
	RCOS	27.01	25.09	33.85	27.31	35.21	30.33	30.78	21.72	28.91
	ASNR	33.29	25.26	35.92	29.74	37.15	31.10	31.12	25.03	31.08
	ALSB	30.72	24.97	32.56	28.41	36.08	30.68	29.96	24.33	29.71
	SGSR	33.44	24.72	34.85	29.42	35.81	30.89	30.51	24.54	30.52
	JASR	34.16	25.18	35.66	29.95	35.88	31.19	31.06	24.95	31.00
	NGS	24.61	24.54	33.39	23.65	34.79	29.60	30.56	20.72	27.73
	PMDSE	24.16	23.06	29.67	22.62	29.41	27.24	25.42	21.57	25.39
GSC- wl_p	34.55	25.28	36.00	30.38	36.92	31.62	31.32	25.06	31.39	
0.3	BCS	25.59	25.00	33.68	23.24	32.85	30.16	29.05	22.19	27.72
	RCOS	30.10	26.42	36.39	29.91	37.10	32.38	32.69	23.96	31.12
	ASNR	36.03	27.09	38.00	31.95	39.04	33.84	32.99	27.68	33.33
	ALSB	35.00	26.83	34.30	30.83	38.34	33.36	32.37	26.61	32.20
	SGSR	35.91	26.80	36.87	31.56	37.37	33.27	32.71	27.33	32.73
	JASR	36.59	27.19	36.83	31.87	38.04	34.05	33.09	27.87	33.19
	NGS	27.28	25.99	35.89	27.61	36.43	32.45	32.90	32.41	30.12
	PMDSE	26.73	24.96	32.31	25.31	32.05	29.09	27.57	24.08	27.76
GSC- wl_p	37.23	27.22	38.30	32.53	39.23	34.29	33.32	27.89	33.75	
0.4	BCS	27.10	26.31	35.66	24.81	34.65	32.06	30.77	23.71	29.38
	RCOS	33.16	27.93	38.25	32.19	38.60	34.31	34.26	25.90	33.07
	ASNR	38.34	28.76	39.78	33.92	40.81	36.09	34.92	30.04	35.33
	ALSB	38.34	29.10	39.60	32.83	40.25	35.47	34.44	28.54	34.58
	SGSR	37.70	28.46	38.63	33.34	38.99	35.68	34.47	29.63	34.61
	JASR	37.39	28.69	38.28	33.96	38.80	36.12	34.70	30.04	34.75
	NGS	30.43	27.59	37.76	30.59	37.82	35.10	34.57	24.65	32.31
	PMDSE	29.74	26.47	34.27	27.66	33.94	30.97	28.94	25.92	29.74
GSC- wl_p	39.13	28.85	40.05	34.42	40.93	36.66	35.00	30.28	35.67	
0.5	BCS	28.67	27.64	37.51	26.20	36.29	33.78	32.31	25.30	30.96
	RCOS	35.36	29.03	39.73	33.82	40.02	36.19	35.89	28.02	34.76
	ASNR	40.24	30.41	41.37	35.68	42.32	38.39	36.42	32.06	37.11
	ALSB	39.26	30.03	41.18	34.81	41.93	37.79	36.21	30.61	36.48
	SGSR	39.38	30.09	40.07	35.28	40.56	37.90	35.97	31.71	36.37
	JASR	40.31	30.30	39.47	35.72	41.44	38.33	36.22	32.04	36.73
	NGS	33.31	29.32	39.41	33.68	39.44	37.21	36.07	26.11	34.32
	PMDSE	31.64	27.70	35.79	29.55	34.79	32.09	30.09	26.95	31.07
GSC- wl_p	40.94	30.52	41.63	36.24	42.38	39.09	36.53	32.46	37.47	

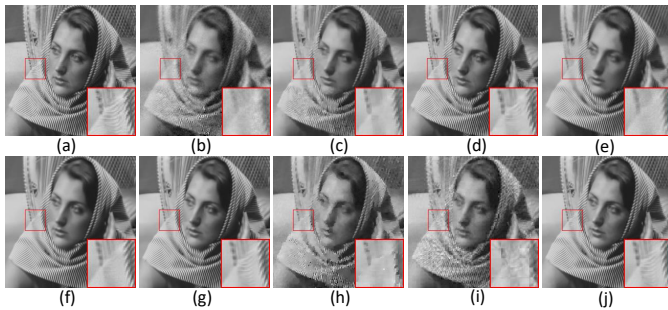


Fig. 10. CS recovery of *Barbara* with $0.2N$ measurements. (a) Original image; (b) BCS [44] (PSNR = 24.24dB); (c) RCOS [52] (PSNR = 27.01dB); (d) ASNR [53] (PSNR = 33.29dB); (e) ALSB [54] (PSNR = 30.72dB); (f) SGSR [55] (PSNR = 33.44dB); (g) JASR [56] (PSNR = 34.16dB); (h) NGS [69] (PSNR = 24.61dB); (i) PMDSE [70] (PSNR = 24.16dB); (j) GSC- wl_p (PSNR = **34.55dB**).

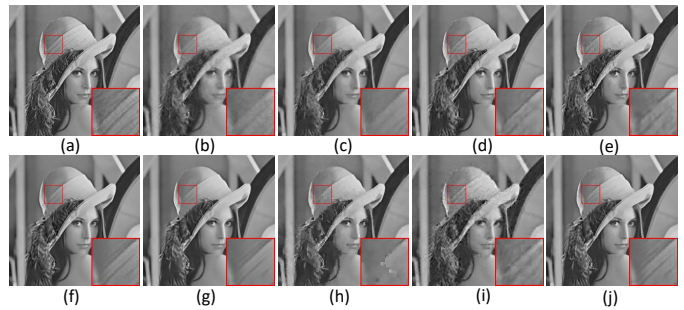


Fig. 11. CS recovery of *Lena* with $0.2N$ measurements. (a) Original image; (b) BCS [44] (PSNR = 28.15dB); (c) RCOS [52] (PSNR = 30.33dB); (d) ASNR [53] (PSNR = 31.10dB); (e) ALSB [54] (PSNR = 30.68dB); (f) SGSR [55] (PSNR = 30.89dB); (g) JASR [56] (PSNR = 31.19dB); (h) NGS [69] (PSNR = 29.60dB); (i) PMDSE [70] (PSNR = 27.24dB); (j) GSC- wl_p (PSNR = **31.62dB**).

6.08dB improvement on average over BCS, RCOS, ASNR, ALSB, SGSR, JASR, NGS and PMDSE methods, respectively. The visual comparisons of image *Barbara* and image *Lena* with $0.2N$ measurements are shown in Fig. 10 and Fig. 11, respectively. One can observe that BCS and PMDSE methods cannot obtain the well perceptual results. Though RCOS, ASNR, ALSB, SGSR, JASR and NGS methods obtain better results than BCS and PMDSE methods, they still suffer from some undesirable visual artifacts or over-smooth effect. The

proposed GSC- wl_p not only removes most of the visual artifacts, but also preserves large-scale sharp edges and small-scale fine image details.

D. Suitable setting of the power p

In this subsection, we discuss how to select the p value for the superior performance of the proposed GSC- wl_p . To be concrete, we randomly select 30 images (size: 256×256) and test the proposed GSC- wl_p with different p values under the

TABLE IX
TESTING THE DIFFERENT POWER p VALUES FOR THE INFLUENCE OF DIFFERENT IMAGE RESTORATION TASKS.

Image Inpainting																				
p	0.05	0.1	0.15	0.2	0.25	0.3	0.35	0.4	0.45	0.5	0.55	0.6	0.65	0.7	0.75	0.8	0.85	0.9	0.95	1
80%	25.69	25.76	25.83	25.89	25.94	25.99	26.02	26.04	26.08	26.07	26.06	26.05	26.03	25.99	25.92	25.82	25.72	25.53	25.38	25.16
70%	28.24	28.30	28.36	28.41	28.45	28.49	28.51	28.54	28.55	28.55	28.48	28.45	28.41	28.35	28.24	28.15	28.01	27.89	27.71	27.44
60%	28.54	28.70	28.84	28.98	29.13	29.26	29.38	29.49	29.58	29.66	29.75	29.82	29.90	29.97	30.04	30.09	30.14	30.18	30.22	30.20
50%	30.53	30.72	30.90	31.07	31.21	31.34	31.47	31.57	31.67	31.76	31.84	31.92	31.99	32.05	32.11	32.15	32.18	32.21	32.23	32.22
Image CS Recovery																				
p	0.05	0.1	0.15	0.2	0.25	0.3	0.35	0.4	0.45	0.5	0.55	0.6	0.65	0.7	0.75	0.8	0.85	0.9	0.95	1
0.2N	28.40	28.48	28.57	28.64	28.72	28.79	28.86	28.91	28.96	29.06	29.04	29.01	28.99	28.98	28.89	28.62	28.50	28.14	27.86	27.67
0.3N	30.40	30.47	30.55	30.63	30.71	30.79	30.88	30.96	31.05	31.14	31.23	31.32	31.41	31.51	31.60	31.68	31.77	31.84	31.95	31.90
0.4N	32.93	33.03	33.12	33.21	33.30	33.38	33.47	33.55	33.64	33.72	33.80	33.87	33.94	34.00	34.05	34.10	34.14	34.17	34.19	34.18
0.5N	34.91	35.01	35.10	35.20	35.30	35.40	35.50	35.59	35.69	35.78	35.86	35.93	35.99	36.05	36.10	36.14	36.16	36.16	36.17	36.16

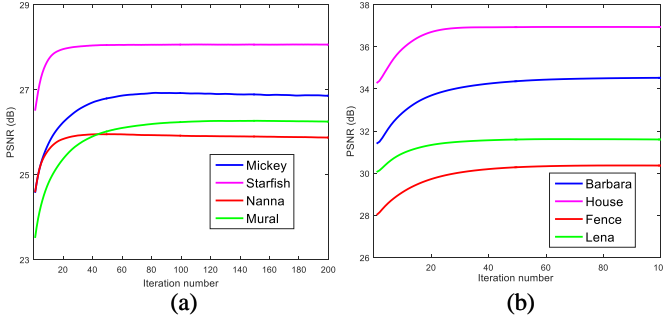


Fig. 12. Convergence analysis of the proposed scheme. (a) PSNR results versus iteration number for image inpainting with 80% pixels missing. (b) PSNR results versus iteration number for image CS recovery with 0.2N measurements.

image inpainting and image CS recovery tasks. Table IX shows the average PSNR results under different p values from 0.05 to 1 with interval 0.05. It can be seen that the best reconstruction performance of the image inpainting task is obtained by setting $p = 0.45, 0.45, 0.95$ and 0.95 when 80%, 70%, 60% and 50% pixels are missing, respectively. Meanwhile, the best CS reconstruction performance of the image CS recovery task is obtained by setting $p = 0.5, 0.95, 0.95$ and 0.95 with $0.2N, 0.3N, 0.4N$ and $0.5N$ measurements, respectively. Therefore, in image inpainting, we choose $p = 0.45, 0.45, 0.95$ and 0.95 when 80%, 70%, 60% and 50% pixels are missing, respectively. In image CS recovery, we choose $p = 0.5, 0.95, 0.95$ and 0.95 with $0.2N, 0.3N, 0.4N$ and $0.5N$ measurements, respectively.

E. Convergence

Since the proposed model is non-convex, it is difficult to provide its theoretical proof of global convergence. Hereby, we present empirical evidence to show the convergence of the proposed model. Fig. 12 plots the curves of the PSNR values versus the iteration numbers for image inpainting with 80% pixels missing for image *Mickey, Starfish, Nanna* and *Murala* as well as image CS recovery (including image *Barbara, House, Fence* and *Lena*) with $0.2N$ measurements, respectively. It can be seen that with the increase of the iteration numbers, the PSNR curves of the reconstructed images gradually increase and then become flat and stable. Therefore, we conclude that the proposed GSC- $w\ell_p$ has a good convergence performance.

VI. CONCLUSION

This paper proposed a benchmark to sparse coding from the perspective of rank minimization. A group-based adaptive

dictionary learning method has been designed to bridge the gap between the GSC and rank minimization models. We have proved the equivalence of the GSC and rank minimization models under the designed dictionary, and thus the sparse coefficients of each patch group were measured by computing the singular values of each patch group. In this way, we have earned a benchmark to measure the sparsity of each patch group since the singular values of the original image patch groups can be easily computed by SVD operator. Then, the proposed benchmark can be used to measure different norm minimization methods in sparse coding through analyzing their corresponding rank minimization methods. To be concrete, four well-known rank minimization methods including NNM, SNM, WNNM and WSNM, have been adopted to analyze the sparsity of each patch group and the solution of WSNM has been found to be the best approximation to real singular values of each patch group. Based on the above analysis, NNM, SNM, WNNM and WSNM can be equivalently transformed into ℓ_1 -norm minimization, ℓ_p -norm minimization, weighted ℓ_1 -norm minimization and the weighted ℓ_p -norm minimization problems in GSC, respectively. Meanwhile, based on the earned benchmark in sparse coding, the weighted ℓ_p -norm minimization was also expected to achieve higher performance than the other three norm minimization methods. To verify the feasibility of the proposed benchmark, we compared the weighted ℓ_p -norm minimization with the other three norm minimization methods in sparse coding. To make the proposed optimization tractable, we have employed the ADMM algorithm to solve the non-convex weighted ℓ_p -norm minimization problem. Experimental results on two applications: image inpainting and image CS recovery, have demonstrated that the proposed scheme is feasible and achieves performance improvements over the state-of-the-art methods both quantitatively and qualitatively.

APPENDIX A

PROOF OF THE LEMMA 2

Proof. The adaptive dictionary \mathbf{D}_i is constructed by Eq. (10). From the unitary property of \mathbf{U}_i and \mathbf{V}_i , we have

$$\begin{aligned}
 \|\mathbf{Y}_i - \mathbf{X}_i\|_F^2 &= \|\mathbf{D}_i(\mathbf{B}_i - \mathbf{A}_i)\|_F^2 = \|\mathbf{U}_i \text{diag}(\mathbf{B}_i - \mathbf{A}_i) \mathbf{V}_i\|_F^2 \\
 &= \text{Tr}(\mathbf{U}_i \text{diag}(\mathbf{B}_i - \mathbf{A}_i) \mathbf{V}_i \mathbf{V}_i^T \text{diag}(\mathbf{B}_i - \mathbf{A}_i) \mathbf{U}_i^T) \\
 &= \text{Tr}(\mathbf{U}_i \text{diag}(\mathbf{B}_i - \mathbf{A}_i) \text{diag}(\mathbf{B}_i - \mathbf{A}_i) \mathbf{U}_i^T) \\
 &= \text{Tr}(\text{diag}(\mathbf{B}_i - \mathbf{A}_i) \mathbf{U}_i \mathbf{U}_i^T \text{diag}(\mathbf{B}_i - \mathbf{A}_i)) \\
 &= \text{Tr}(\text{diag}(\mathbf{B}_i - \mathbf{A}_i) \text{diag}(\mathbf{B}_i - \mathbf{A}_i)) \\
 &= \|\mathbf{B}_i - \mathbf{A}_i\|_F^2,
 \end{aligned} \tag{38}$$

where $\mathbf{X}_i = \mathbf{D}_i \mathbf{A}_i$ and $\mathbf{Y}_i = \mathbf{D}_i \mathbf{B}_i$. □

APPENDIX B
PROOF OF THE THEOREM 2

Proof. On the basis of Lemma 2, we have

$$\begin{aligned} \hat{\mathbf{A}}_i &= \arg \min_{\mathbf{A}_i} \left(\frac{1}{2} \|\mathbf{Y}_i - \mathbf{D}_i \mathbf{A}_i\|_F^2 + \lambda \|\mathbf{A}_i\|_1 \right) \\ &= \arg \min_{\mathbf{A}_i} \left(\frac{1}{2} \|\mathbf{B}_i - \mathbf{A}_i\|_F^2 + \lambda \|\mathbf{A}_i\|_1 \right) \\ &= \arg \min_{\boldsymbol{\alpha}_i} \left(\frac{1}{2} \|\boldsymbol{\beta}_i - \boldsymbol{\alpha}_i\|_2^2 + \lambda \|\boldsymbol{\alpha}_i\|_1 \right), \end{aligned} \quad (39)$$

where $\mathbf{X}_i = \mathbf{D}_i \mathbf{A}_i$ and $\mathbf{Y}_i = \mathbf{D}_i \mathbf{B}_i$. $\boldsymbol{\alpha}_i$ and $\boldsymbol{\beta}_i$ denote the vectorization of the matrix \mathbf{A}_i and \mathbf{B}_i , respectively.

Therefore, based on Lemma 1, we have

$$\boldsymbol{\alpha}_i = \text{soft}(\boldsymbol{\beta}_i, \lambda) = \text{sgn}(\boldsymbol{\beta}_i) \odot \max(\text{abs}(\boldsymbol{\beta}_i) - \lambda, 0). \quad (40)$$

Obviously, according to Eqs. (9) and (10), we have

$$\begin{aligned} \mathbf{D}_i \hat{\mathbf{A}}_i &= \sum_{j=1}^{n_1} \text{soft}(\boldsymbol{\beta}_{i,j}, \lambda) \mathbf{d}_{i,j} \\ &= \sum_{j=1}^{n_1} \text{soft}(\boldsymbol{\beta}_{i,j}, \lambda) \mathbf{u}_{i,j} \mathbf{v}_{i,j}^T \\ &= \mathbf{U}_i \mathcal{D}_\lambda(\boldsymbol{\Delta}_i) \mathbf{V}_i^T = \mathcal{D}_\lambda(\mathbf{Y}_i), \end{aligned} \quad (41)$$

where $\boldsymbol{\beta}_{i,j}$ represents the j -th element of the i -th group sparse coefficient $\boldsymbol{\beta}_i$, and $\boldsymbol{\Delta}_i$ is the singular value matrix of the i -th group \mathbf{Y}_i .

Following this, and based on Theorem 1, we have proved that the ℓ_1 -norm minimization based GSC problem is equivalent to the NNM problem, *i.e.*,

$$\begin{aligned} \hat{\mathbf{A}}_i &= \arg \min_{\mathbf{A}_i} \left(\frac{1}{2} \|\mathbf{Y}_i - \mathbf{D}_i \mathbf{A}_i\|_F^2 + \lambda \|\mathbf{A}_i\|_1 \right) \\ &\quad \Updownarrow \\ \hat{\mathbf{X}}_i &= \arg \min_{\mathbf{X}_i} \left(\frac{1}{2} \|\mathbf{Y}_i - \mathbf{X}_i\|_F^2 + \lambda \|\mathbf{X}_i\|_* \right). \end{aligned} \quad (42)$$

APPENDIX C

PROOF OF THE COROLLARY 1

Proof. We first prove the weighted ℓ_1 -norm minimization based GSC problem is equivalent to the weighted nuclear norm minimization (WNNM) problem. Specifically, the weighted norm $\|\mathbf{X}\|_{\mathbf{w},*}$ is used to regularize \mathbf{X} and Eq. (2) can be rewritten as

$$\hat{\mathbf{X}} = \arg \min_{\mathbf{X}} \left(\frac{1}{2} \|\mathbf{Y} - \mathbf{X}\|_F^2 + \|\mathbf{X}\|_{\mathbf{w},*} \right). \quad (43)$$

In order to prove that the equivalence of the weighted ℓ_1 -norm minimization based GSC problem and the WNNM problem, we firstly give the following lemma and theorems.

Lemma 3. *For the following optimization problem*

$$\min_{\mathbf{x}_i} \sum_{i=1}^n \left(\frac{1}{2} (a_i - x_i)^2 + w_i x_i \right), \quad (44)$$

then the global optimum of Eq. (44) is $\hat{x}_i = \text{soft}(a_i, w_i) = \max(a_i - w_i, 0)$.

□ *Proof.* See [38]. □

Theorem 4. *If the singular values $\delta_1 \geq \dots \geq \delta_{n_1}$ and the weights satisfy $0 \leq w_1 \leq \dots \leq w_{n_1}$, $n_1 = \min(d, m)$, the WNNM problem in Eq. (43) has a globally optimal solution,*

$$\hat{\mathbf{X}} = \mathbf{U} \mathcal{D}_{\mathbf{w}}(\boldsymbol{\Delta}) \mathbf{V}^T, \quad (45)$$

where $\mathbf{Y} = \mathbf{U} \boldsymbol{\Delta} \mathbf{V}^T$ is the SVD of \mathbf{Y} and $\mathcal{D}_{\mathbf{w}}(\boldsymbol{\Delta})$ is the generalized soft-thresholding operator with the weighted vector \mathbf{w} , *i.e.*, $\mathcal{D}_{\mathbf{w}}(\boldsymbol{\Delta})_i = \text{soft}(\boldsymbol{\Delta}_i, w_i) = \max(\boldsymbol{\Delta}_i - w_i, 0)$, where $\boldsymbol{\Delta}_i$ denotes the i -th singular value of $\boldsymbol{\Delta}$.

Proof. See [25]. □

Theorem 5. *For $0 \leq w_1 \leq \dots \leq w_{n_1}$ and $\mathbf{Y} \in \mathbb{R}^{d \times m}$, $n_1 = \min(d, m)$, the singular value shrinkage operator Eq. (45) satisfies Eq. (43).*

Proof. See [61]. □

Then, for each patch group \mathbf{X}_i in \mathbf{X} , the WNNM problem in Eq. (43) can be rewritten as

$$\hat{\mathbf{X}}_i = \arg \min_{\mathbf{X}_i} \left(\frac{1}{2} \|\mathbf{Y}_i - \mathbf{X}_i\|_F^2 + \|\mathbf{X}_i\|_{\mathbf{w}_i,*} \right). \quad (46)$$

For the weighted ℓ_1 -norm minimization based GSC problem and based on Lemma 2, we have,

$$\begin{aligned} \hat{\mathbf{A}}_i &= \arg \min_{\mathbf{A}_i} \left(\frac{1}{2} \|\mathbf{Y}_i - \mathbf{D}_i \mathbf{A}_i\|_F^2 + \|\mathbf{W}_i \circ \mathbf{A}_i\|_1 \right) \\ &= \arg \min_{\mathbf{A}_i} \left(\frac{1}{2} \|\mathbf{B}_i - \mathbf{A}_i\|_F^2 + \|\mathbf{W}_i \circ \mathbf{A}_i\|_1 \right) \\ &= \arg \min_{\boldsymbol{\alpha}_i} \left(\frac{1}{2} \|\boldsymbol{\beta}_i - \boldsymbol{\alpha}_i\|_2^2 + \|\mathbf{w}_i \boldsymbol{\alpha}_i\|_1 \right), \end{aligned} \quad (47)$$

where \circ represents the element-wise product of two matrices (Hadamard product). $\mathbf{X}_i = \mathbf{D}_i \mathbf{A}_i$ and $\mathbf{Y}_i = \mathbf{D}_i \mathbf{B}_i$. $\boldsymbol{\alpha}_i$, $\boldsymbol{\beta}_i$ and \mathbf{w}_i denote the vectorization of the matrix \mathbf{A}_i , \mathbf{B}_i and \mathbf{W}_i , respectively.

□ Then, based on Lemma 3, we have,

$$\boldsymbol{\alpha}_i = \text{soft}(\boldsymbol{\beta}_i, \mathbf{w}_i) = \max(\boldsymbol{\beta}_i - \mathbf{w}_i, 0). \quad (48)$$

Based on Eqs. (9) and (10), we have

$$\begin{aligned} \hat{\mathbf{X}}_i &= \mathbf{D}_i \hat{\mathbf{A}}_i = \sum_{j=1}^{n_1} \text{soft}(\boldsymbol{\beta}_{i,j}, w_{i,j}) \mathbf{d}_{i,j} \\ &= \sum_{j=1}^{n_1} \text{soft}(\boldsymbol{\beta}_{i,j}, w_{i,j}) \mathbf{u}_{i,j} \mathbf{v}_{i,j}^T \\ &= \mathbf{U}_i \mathcal{D}_{\mathbf{w}_i}(\boldsymbol{\Delta}_i) \mathbf{V}_i^T. \end{aligned} \quad (49)$$

Therefore, based on Theorem 5, we prove that the weighted ℓ_1 -norm minimization based GSC problem is equivalent to the WNNM problem, *i.e.*,

$$\begin{aligned} \hat{\mathbf{A}}_i &= \arg \min_{\mathbf{A}_i} \left(\frac{1}{2} \|\mathbf{Y}_i - \mathbf{D}_i \mathbf{A}_i\|_F^2 + \|\mathbf{W}_i \circ \mathbf{A}_i\|_1 \right) \\ &\quad \Updownarrow \\ \hat{\mathbf{X}}_i &= \arg \min_{\mathbf{X}_i} \left(\frac{1}{2} \|\mathbf{Y}_i - \mathbf{X}_i\|_F^2 + \|\mathbf{X}_i\|_{\mathbf{w}_i,*} \right). \end{aligned} \quad (50)$$

Note that here we assume the setting of the weight \mathbf{W}_i in Eq. (46) is as the same as the weight \mathbf{W}_i in Eq. (47).

Next, we prove the ℓ_p -norm minimization based GSC problem is equivalent to the Schatten p -norm minimization (SNM) problem. Specifically, the Schatten p -norm $\|\mathbf{X}_i\|_{S_p}$ is used to regularize \mathbf{X}_i in Eq. (2) and for each patch group \mathbf{X}_i , we have,

$$\hat{\mathbf{X}}_i = \min_{\mathbf{X}_i} \left(\frac{1}{2} \|\mathbf{Y}_i - \mathbf{X}_i\|_F^2 + \lambda \|\mathbf{X}_i\|_{S_p} \right). \quad (51)$$

To prove that the equivalence of the ℓ_p -norm minimization based GSC problem and the SNM problem, we firstly give the following theorem.

Theorem 6. *Let $\mathbf{Y}_i = \mathbf{U}_i \mathbf{\Delta}_i \mathbf{V}_i^T$ be the SVD of $\mathbf{Y}_i \in \mathbb{R}^{d \times m}$ and $\mathbf{\Delta}_i = \text{diag}(\delta_{i,1}, \dots, \delta_{i,n_1})$, $n_1 = \min(d, m)$. The optimal solution \mathbf{X}_i to problem Eq. (51) is $\mathbf{U}_i \mathbf{\Sigma}_i \mathbf{V}_i^T$, where $\mathbf{\Sigma}_i = \text{diag}(\sigma_{i,1}, \dots, \sigma_{i,n_1})$. Then the solution of the j -th diagonal element $\sigma_{i,j}$ of the diagonal matrix $\mathbf{\Sigma}_i$ is solved by the following problem,*

$$\min_{\sigma_{i,j}} \left(\frac{1}{2} (\delta_{i,j} - \sigma_{i,j})^2 + \lambda \sigma_{i,j}^p \right), \quad (52)$$

where $\sigma_{i,j}$ represents the j -th singular value of each data matrix \mathbf{X}_i .

Proof. See [24]. \square

Now, for the ℓ_p -norm minimization based GSC problem, and based on Lemma 2, we have,

$$\begin{aligned} \hat{\mathbf{A}}_i &= \arg \min_{\mathbf{A}_i} \left(\frac{1}{2} \|\mathbf{Y}_i - \mathbf{D}_i \mathbf{A}_i\|_F^2 + \lambda \|\mathbf{A}_i\|_p \right) \\ &= \arg \min_{\mathbf{A}_i} \left(\frac{1}{2} \|\mathbf{B}_i - \mathbf{A}_i\|_F^2 + \lambda \|\mathbf{A}_i\|_p \right) \\ &= \arg \min_{\boldsymbol{\alpha}_i} \left(\frac{1}{2} \|\boldsymbol{\beta}_i - \boldsymbol{\alpha}_i\|_2^2 + \lambda \|\boldsymbol{\alpha}_i\|_p \right), \end{aligned} \quad (53)$$

where $\mathbf{X}_i = \mathbf{D}_i \mathbf{A}_i$ and $\mathbf{Y}_i = \mathbf{D}_i \mathbf{B}_i$. $\boldsymbol{\alpha}_i$ and $\boldsymbol{\beta}_i$ denote the vectorization of the matrix \mathbf{A}_i and \mathbf{B}_i , respectively.

Then the solution of the j -th element $\alpha_{i,j}$ of $\boldsymbol{\alpha}_i$ in Eq. (53) is solved by the following minimization problem,

$$\min_{\alpha_{i,j}} \left(\frac{1}{2} (\beta_{i,j} - \alpha_{i,j})^2 + \lambda \alpha_{i,j}^p \right). \quad (54)$$

Obviously, based on the designed adaptive dictionary \mathbf{D}_i in Eq. (10), Eq. (54) is equivalent to Eq. (52).

Therefore, we prove that the ℓ_p -norm minimization based GSC problem is equivalent to the SNM problem, *i.e.*,

$$\begin{aligned} \hat{\mathbf{A}}_i &= \arg \min_{\mathbf{A}_i} \left(\frac{1}{2} \|\mathbf{Y}_i - \mathbf{D}_i \mathbf{A}_i\|_F^2 + \lambda \|\mathbf{A}_i\|_p \right) \\ &\quad \Updownarrow \\ \hat{\mathbf{X}}_i &= \arg \min_{\mathbf{X}_i} \left(\frac{1}{2} \|\mathbf{Y}_i - \mathbf{X}_i\|_F^2 + \lambda \|\mathbf{X}_i\|_{S_p} \right). \end{aligned} \quad (55)$$

Similar to the ℓ_p -norm minimization based GSC problem is equivalent to the SNM problem, we can also prove that the weighted ℓ_p -norm minimization based GSC problem is

equivalent to the weighted Schatten p -norm minimization (WSNM) problem, *i.e.*,

$$\begin{aligned} \hat{\mathbf{A}}_i &= \arg \min_{\mathbf{A}_i} \left(\frac{1}{2} \|\mathbf{Y}_i - \mathbf{D}_i \mathbf{A}_i\|_F^2 + \|\mathbf{W}_i \circ \mathbf{A}_i\|_p \right) \\ &\quad \Updownarrow \\ \hat{\mathbf{X}}_i &= \arg \min_{\mathbf{X}_i} \left(\frac{1}{2} \|\mathbf{Y}_i - \mathbf{X}_i\|_F^2 + \|\mathbf{X}_i\|_{\mathbf{w}_i, S_p} \right). \end{aligned} \quad (56)$$

Therefore, based on the above analysis, we prove the Corollary 1. \square

ACKNOWLEDGMENT

The authors would like to appreciate the associate editor for coordinating the review of the manuscript, and appreciate the anonymous reviewers for their constructive suggestions to improve the manuscript.

REFERENCES

- [1] M. Aharon, M. Elad, and A. Bruckstein, "k-svd: An algorithm for designing overcomplete dictionaries for sparse representation," *IEEE Transactions on signal processing*, vol. 54, no. 11, pp. 4311–4322, 2006.
- [2] M. Elad and M. Aharon, "Image denoising via sparse and redundant representations over learned dictionaries," *IEEE Transactions on Image processing*, vol. 15, no. 12, pp. 3736–3745, 2006.
- [3] J. Mairal, F. Bach, J. Ponce, and G. Sapiro, "Online dictionary learning for sparse coding," in *International Conference on Machine Learning*. ACM, 2009, pp. 689–696.
- [4] J. Mairal, J. Ponce, G. Sapiro, A. Zisserman, and F. R. Bach, "Supervised dictionary learning," in *Advances in neural information processing systems*, 2009, pp. 1033–1040.
- [5] J. Zhang, D. Zhao, and W. Gao, "Group-based sparse representation for image restoration," *IEEE Transactions on Image Processing*, vol. 23, no. 8, pp. 3336–3351, 2014.
- [6] W. Dong, G. Shi, Y. Ma, and X. Li, "Image restoration via simultaneous sparse coding: Where structured sparsity meets gaussian scale mixture," *International Journal of Computer Vision*, vol. 114, no. 2-3, pp. 217–232, 2015.
- [7] Q. Wang, X. Zhang, Y. Wu, L. Tang, and Z. Zha, "Nonconvex weighted ℓ_p minimization based group sparse representation framework for image denoising," *IEEE Signal Processing Letters*, vol. 24, no. 11, pp. 1686–1690, 2017.
- [8] J. Mairal, F. Bach, J. Ponce, G. Sapiro, and A. Zisserman, "Non-local sparse models for image restoration," in *IEEE Conference on Computer Vision*. IEEE, 2009, pp. 2272–2279.
- [9] J. Xu, L. Zhang, W. Zuo, D. Zhang, and X. Feng, "Patch group based nonlocal self-similarity prior learning for image denoising," in *IEEE international conference on computer vision*, 2015, pp. 244–252.
- [10] S. Li, H. Yin, and L. Fang, "Group-sparse representation with dictionary learning for medical image denoising and fusion," *IEEE Transactions on biomedical engineering*, vol. 59, no. 12, pp. 3450–3459, 2012.
- [11] S. Gao, L.-T. Chia, I. W.-H. Tsang, and Z. Ren, "Concurrent single-label image classification and annotation via efficient multi-layer group sparse coding," *IEEE Transactions on Multimedia*, vol. 16, no. 3, pp. 762–771, 2014.
- [12] Y. Sun, Q. Liu, J. Tang, and D. Tao, "Learning discriminative dictionary for group sparse representation," *IEEE Transactions on Image Processing*, vol. 23, no. 9, pp. 3816–3828, 2014.
- [13] J. Liu, W. Yang, X. Zhang, and Z. Guo, "Retrieval compensated group structured sparsity for image super-resolution," *IEEE Transactions on Multimedia*, vol. 19, no. 2, pp. 302–316, 2016.
- [14] J. M. Keller, M. R. Gray, and J. A. Givens, "A fuzzy k-nearest neighbor algorithm," *IEEE transactions on systems, man, and cybernetics*, no. 4, pp. 580–585, 1985.
- [15] D. L. Donoho, "For most large underdetermined systems of linear equations the minimal ℓ_1 -norm solution is also the sparsest solution," *Communications on pure and applied mathematics*, vol. 59, no. 6, pp. 797–829, 2006.
- [16] E. J. Candes, M. B. Wakin, and S. P. Boyd, "Enhancing sparsity by reweighted ℓ_1 minimization," *Journal of Fourier analysis and applications*, vol. 14, no. 5, pp. 877–905, 2008.

- [17] Z. Xu, X. Chang, F. Xu, and H. Zhang, " $l_{1/2}$ regularization: A thresholding representation theory and a fast solver," *IEEE Transactions on Neural Networks and Learning Systems*, vol. 23, no. 7, pp. 1013–1027, July 2012.
- [18] X. Liao, H. Li, and L. Carin, "Generalized alternating projection for weighted-2,1 minimization with applications to model-based compressive sensing," *SIAM Journal on Imaging Sciences*, vol. 7, no. 2, pp. 797–823, 2014.
- [19] E. J. Candès and B. Recht, "Exact matrix completion via convex optimization," *Foundations of Computational mathematics*, vol. 9, no. 6, p. 717, 2009.
- [20] R. Chartrand and B. Wohlberg, "A nonconvex admm algorithm for group sparsity with sparse groups," in *IEEE International Conference on Acoustics, Speech and Signal Processing*. IEEE, 2013, pp. 6009–6013.
- [21] D. Krishnan and R. Fergus, "Fast image deconvolution using hyper-laplacian priors," in *Advances in Neural Information Processing Systems*, 2009, pp. 1033–1041.
- [22] Q. Lyu, Z. Lin, Y. She, and C. Zhang, "A comparison of typical ℓ_p minimization algorithms," *Neurocomputing*, vol. 119, pp. 413–424, 2013.
- [23] J.-F. Cai, E. J. Candès, and Z. Shen, "A singular value thresholding algorithm for matrix completion," *SIAM Journal on Optimization*, vol. 20, no. 4, pp. 1956–1982, 2010.
- [24] F. Nie, H. Wang, H. Huang, and C. Ding, "Joint Schatten p -norm and ℓ_p -norm robust matrix completion for missing value recovery," *Knowledge and Information Systems*, vol. 42, no. 3, pp. 525–544, 2015.
- [25] S. Gu, L. Zhang, W. Zuo, and X. Feng, "Weighted nuclear norm minimization with application to image denoising," in *IEEE Conference on Computer Vision and Pattern Recognition*, 2014, pp. 2862–2869.
- [26] Y. Xie, S. Gu, Y. Liu, W. Zuo, W. Zhang, and L. Zhang, "Weighted Schatten p -norm minimization for image denoising and background subtraction," *IEEE transactions on image processing*, vol. 25, no. 10, pp. 4842–4857, 2016.
- [27] C. Lu, C. Zhu, C. Xu, S. Yan, and Z. Lin, "Generalized singular value thresholding," in *Proceedings of the AAAI Conference on Artificial Intelligence*, 2015, pp. 1805–1811.
- [28] Z. Kang, C. Peng, and Q. Cheng, "Robust pca via nonconvex rank approximation," in *IEEE International Conference on Data Mining*. IEEE, 2015, pp. 211–220.
- [29] Y. Hu, D. Zhang, J. Ye, X. Li, and X. He, "Fast and accurate matrix completion via truncated nuclear norm regularization," *IEEE transactions on pattern analysis and machine intelligence*, vol. 35, no. 9, pp. 2117–2130, 2013.
- [30] T.-H. Oh, Y.-W. Tai, J.-C. Bazin, H. Kim, and I. S. Kweon, "Partial sum minimization of singular values in robust pca: Algorithm and applications," *IEEE transactions on pattern analysis and machine intelligence*, vol. 38, no. 4, pp. 744–758, 2016.
- [31] A. Parekh and I. W. Selesnick, "Enhanced low-rank matrix approximation," *IEEE Signal Processing Letters*, vol. 23, no. 4, pp. 493–497, 2016.
- [32] M. Li, J. Liu, Z. Xiong, X. Sun, and Z. Guo, "Marlow: A joint multi-planar autoregressive and low-rank approach for image completion," in *European Conference on Computer Vision*. Springer, 2016, pp. 819–834.
- [33] Z. Zha, X. Liu, X. Huang, H. Shi, Y. Xu, Q. Wang, L. Tang, and X. Zhang, "Analyzing the group sparsity based on the rank minimization methods," in *IEEE International Conference on Multimedia and Expo*, July 2017, pp. 883–888.
- [34] A. Eriksson and A. Van Den Hengel, "Efficient computation of robust low-rank matrix approximations in the presence of missing data using the l_1 norm," in *IEEE international conference on computer vision*. IEEE, 2010, pp. 771–778.
- [35] G. Liu, Z. Lin, S. Yan, J. Sun, Y. Yu, and Y. Ma, "Robust recovery of subspace structures by low-rank representation," *IEEE Transactions on Pattern Analysis and Machine Intelligence*, vol. 35, no. 1, pp. 171–184, 2013.
- [36] Q. Zhao, D. Meng, Z. Xu, W. Zuo, and Y. Yan, " ℓ_1 -norm low-rank matrix factorization by variational bayesian method," *IEEE transactions on neural networks and learning systems*, vol. 26, no. 4, pp. 825–839, 2015.
- [37] Y. Chang, L. Yan, and S. Zhong, "Hyper-laplacian regularized unidirectional low-rank tensor recovery for multispectral image denoising," in *IEEE Conference on Computer Vision and Pattern Recognition*, 2017, pp. 4260–4268.
- [38] S. Gu, Q. Xie, D. Meng, W. Zuo, X. Feng, and L. Zhang, "Weighted nuclear norm minimization and its applications to low level vision," *International journal of computer vision*, vol. 121, no. 2, pp. 183–208, 2017.
- [39] T. Blumensath and M. E. Davies, "Iterative hard thresholding for compressed sensing," *Applied and computational harmonic analysis*, vol. 27, no. 3, pp. 265–274, 2009.
- [40] J. A. Tropp and A. C. Gilbert, "Signal recovery from random measurements via orthogonal matching pursuit," *IEEE Transactions on information theory*, vol. 53, no. 12, pp. 4655–4666, 2007.
- [41] C. Li, W. Yin, and Y. Zhang, "Users guide for tval3: Tv minimization by augmented lagrangian and alternating direction algorithms," *CAAM report*, vol. 20, pp. 46–47, 2009.
- [42] W. Hu, G. Cheung, A. Ortega, and O. C. Au, "Multiresolution graph fourier transform for compression of piecewise smooth images," *IEEE Transactions on Image Processing*, vol. 24, no. 1, pp. 419–433, 2015.
- [43] W. Dong, L. Zhang, G. Shi, and X. Li, "Nonlocally centralized sparse representation for image restoration," *IEEE Transactions on Image Processing*, vol. 22, no. 4, pp. 1620–1630, 2013.
- [44] S. Mun and J. E. Fowler, "Block compressed sensing of images using directional transforms," in *IEEE International Conference on Image Processing*. IEEE, 2009, pp. 3021–3024.
- [45] J. Liu, S. Yang, Y. Fang, and Z. Guo, "Structure-guided image inpainting using homography transformation," *IEEE Transactions on Multimedia*, vol. 20, no. 12, pp. 3252–3265, 2018.
- [46] X. Liu, G. Cheung, X. Wu, and D. Zhao, "Random walk graph laplacian-based smoothness prior for soft decoding of jpeg images," *IEEE Transactions on Image Processing*, vol. 26, no. 2, pp. 509–524, 2016.
- [47] M. V. Afonso, J. M. Bioucas-Dias, and M. A. Figueiredo, "An augmented lagrangian approach to the constrained optimization formulation of imaging inverse problems," *IEEE Transactions on Image Processing*, vol. 20, no. 3, pp. 681–695, 2011.
- [48] M. Zhou, H. Chen, J. Paisley, L. Ren, L. Li, Z. Xing, D. Dunson, G. Sapiro, and L. Carin, "Nonparametric bayesian dictionary learning for analysis of noisy and incomplete images," *IEEE Transactions on Image Processing*, vol. 21, no. 1, pp. 130–144, 2012.
- [49] I. Ram, M. Elad, and I. Cohen, "Image processing using smooth ordering of its patches," *IEEE transactions on image processing*, vol. 22, no. 7, pp. 2764–2774, 2013.
- [50] J. Zhang, D. Zhao, R. Xiong, S. Ma, and W. Gao, "Image restoration using joint statistical modeling in a space-transform domain," *IEEE Transactions on Circuits and Systems for Video Technology*, vol. 24, no. 6, pp. 915–928, 2014.
- [51] K. H. Jin and J. C. Ye, "Annihilating filter-based low-rank hankel matrix approach for image inpainting," *IEEE Transactions on Image Processing*, vol. 24, no. 11, pp. 3498–3511, 2015.
- [52] J. Zhang, D. Zhao, C. Zhao, R. Xiong, S. Ma, and W. Gao, "Image compressive sensing recovery via collaborative sparsity," *IEEE Journal on Emerging and Selected Topics in Circuits and Systems*, vol. 2, no. 3, pp. 380–391, Sept 2012.
- [53] Z. Zha, X. Liu, X. Zhang, Y. Chen, L. Tang, Y. Bai, Q. Wang, and Z. Shang, "Compressed sensing image reconstruction via adaptive sparse nonlocal regularization," *The Visual Computer*, vol. 34, no. 1, pp. 117–137, Jan 2018.
- [54] J. Zhang, C. Zhao, D. Zhao, and W. Gao, "Image compressive sensing recovery using adaptively learned sparsifying basis via l_0 minimization," *Signal Processing*, vol. 103, pp. 114–126, 2014.
- [55] J. Zhang, D. Zhao, F. Jiang, and W. Gao, "Structural group sparse representation for image compressive sensing recovery," in *Data Compression Conference*. IEEE, 2013, pp. 331–340.
- [56] N. Eslahi and A. Aghagolzadeh, "Compressive sensing image restoration using adaptive curvelet thresholding and nonlocal sparse regularization," *IEEE Transactions on Image Processing*, vol. 25, no. 7, pp. 3126–3140, 2016.
- [57] X. Liu, D. Zhai, J. Zhou, S. Wang, D. Zhao, and H. Gao, "Sparsity-based image error concealment via adaptive dual dictionary learning and regularization," *IEEE Transactions on Image Processing*, vol. 26, no. 2, pp. 782–796, 2016.
- [58] B. He, L.-Z. Liao, D. Han, and H. Yang, "A new inexact alternating directions method for monotone variational inequalities," *Mathematical Programming*, vol. 92, no. 1, pp. 103–118, 2002.
- [59] S. Boyd, N. Parikh, E. Chu, B. Peleato, and J. Eckstein, "Distributed optimization and statistical learning via the alternating direction method of multipliers," *Foundations and Trends® in Machine Learning*, vol. 3, no. 1, pp. 1–122, 2011.
- [60] C. Zhao, J. Zhang, S. Ma, and W. Gao, "Nonconvex l_p nuclear norm based admm framework for compressed sensing," in *Data Compression Conference*. IEEE, 2016, pp. 161–170.
- [61] W. Dong, G. Shi, X. Li, Y. Ma, and F. Huang, "Compressive sensing

- via nonlocal low-rank regularization," *IEEE Transactions on Image Processing*, vol. 23, no. 8, pp. 3618–3632, 2014.
- [62] C. Zhao, J. Zhang, S. Ma, X. Fan, Y. Zhang, and W. Gao, "Reducing image compression artifacts by structural sparse representation and quantization constraint prior," *IEEE Transactions on Circuits and Systems for Video Technology*, vol. 27, no. 10, pp. 2057–2071, 2017.
- [63] P. Deift and X. Zhou, "A steepest descent method for oscillatory riemann–hilbert problems. asymptotics for the mkdv equation," *Annals of Mathematics*, pp. 295–368, 1993.
- [64] W. Zuo, D. Meng, L. Zhang, X. Feng, and D. Zhang, "A generalized iterated shrinkage algorithm for non-convex sparse coding," in *IEEE international conference on computer vision*, 2013, pp. 217–224.
- [65] S. G. Chang, B. Yu, and M. Vetterli, "Adaptive wavelet thresholding for image denoising and compression," *IEEE transactions on image processing*, vol. 9, no. 9, pp. 1532–1546, 2000.
- [66] L. Zhang, L. Zhang, X. Mou, and D. Zhang, "Fsim: A feature similarity index for image quality assessment," *IEEE transactions on Image Processing*, vol. 20, no. 8, pp. 2378–2386, 2011.
- [67] L. Zhang, Y. Shen, and H. Li, "Vsi: A visual saliency-induced index for perceptual image quality assessment," *IEEE Transactions on Image Processing*, vol. 23, no. 10, pp. 4270–4281, 2014.
- [68] J. G. Serra, M. Testa, R. Molina, and A. K. Katsaggelos, "Bayesian k-svd using fast variational inference," *IEEE Transactions on Image Processing*, vol. 26, no. 7, pp. 3344–3359, July 2017.
- [69] H. Liu, R. Xiong, X. Zhang, Y. Zhang, S. Ma, and W. Gao, "Nonlocal gradient sparsity regularization for image restoration," *IEEE Transactions on Circuits and Systems for Video Technology*, vol. 27, no. 9, pp. 1909–1921, Sept 2017.
- [70] J. Wu, F. Cao, and J. Yin, "Nonlocally multi-morphological representation for image reconstruction from compressive measurements," *IEEE Transactions on Image Processing*, vol. 26, no. 12, pp. 5730–5742, Dec 2017.
- [71] K. Zhang, W. Zuo, S. Gu, and L. Zhang, "Learning deep cnn denoiser prior for image restoration," in *IEEE conference on computer vision and pattern recognition*, 2017, pp. 3929–3938.
- [72] T. Tirer and R. Giryes, "Image restoration by iterative denoising and backward projections," *IEEE Transactions on Image Processing*, vol. 28, no. 3, pp. 1220–1234, March 2019.